

AD-A278 498



1

AFIT/GA/ENY/94M-1

DTIC
ELECTE
APR 22 1994
S F D

COMPRESSION OF A RADAR TRACK OF A NEAR EARTH
SATELLITE INTO AN EARTH CENTERED INERTIAL STATE
VECTOR USING LEAST SQUARES DIFFERENTIAL
CORRECTION

THESIS
Garry Lee Hall
Captain, USAF

AFIT/GA/ENY/94M-1

94-12279



Approved for public release; distribution unlimited

94 4 21 060

AFIT/GA/ENY/94M-1

**COMPRESSION OF A RADAR TRACK OF A NEAR EARTH SATELLITE INTO AN
EARTH CENTERED INERTIAL STATE VECTOR USING LEAST SQUARES
DIFFERENTIAL CORRECTION**

THESIS

Presented to the Faculty of the Graduate School of Engineering

of the Air Force Institute of Technology

Air University

In Partial Fulfillment of the

Requirements for the Degree of

Master of Science in Astronautical Engineering

Garry L. Hall, B.S.

Captain, USAF

March 1994

Accession For	
NTIS CRA&I	<input checked="checked" type="checkbox"/>
DTIC TAB	<input type="checkbox"/>
Unannounced	<input type="checkbox"/>
Justification	
By _____	
Distribution /	
Availability Codes	
Dist	Avail and/or Special
A-1	

Approved for public release; distribution unlimited

Preface

Like most of my peers, I have long been interested in space and most anything related to space exploration and utilization. After being assigned to first Air Force Space Command and then United States Space Command, I found that I enjoyed studying how objects travel through space and especially how to track and predict their movements around the earth. So it was very satisfying to be able to work on a project that has both theoretical and practical applications.

As an orbital analyst at the Space Surveillance Center in Cheyenne Mountain, I routinely tracked objects and updated their predicted positions but I could not have explained how the mathematics worked. Through the classes in Orbital Dynamics taught here at AFIT, I learned the theory of how orbits could be estimated using observations. But it was the research for this thesis, the development of programs to simulate the orbit of a satellite and to generate radar observations and the use of these observations to estimate the state of the satellite, that fully developed the level of understanding that I desired. This project has been both difficult and challenging, but few worthwhile endeavors are not.

I could not have completed this work without the help and encouragement of my teachers, friends and family. I would like to thank Dr. Wiesel for his patience and understanding as well as for his insight and direction when things got tough. I would also like to thank my fellow classmates, especially Captain Tony Nash, for answering my many questions and for simply listening to my ideas. And last, but certainly not least, my wife who suffered through the entire process with me.

Table of Contents

	Page
Preface.....	ii
List of Figures.....	vi
List of Tables.....	viii
Abstract.....	ix
I. Background and Statement of the Problem	1
1.1 Introduction	1
1.2 Problem Statement	2
1.3 Research Objectives.....	3
1.4 Research Questions	3
1.5 Assumptions.....	4
1.6 Scope	5
1.7 Summary.....	5
II. Theoretical Background	6
2.1 Introduction	6
2.2 The Method of Least Squares	7
2.3 Multi-Dimensional Least Squares.....	9
2.4 Linearizing the Problem	10
2.5 Correcting the Reference State	12
2.6 Implementing Least Squares on a Computer.....	14
2.7 Summary.....	15
III. Methodology.....	16
3.1 Introduction	16

	Page
3.2 The Truth Model.....	16
3.2.1 Program Execution	16
3.2.2 The Equations of Motion	18
3.2.3 Program Validation	21
3.3 The Estimator	21
3.3.1 Program Execution	22
3.3.2 Development of the Taylor Series Approximations.....	24
3.3.3 Program Validation	26
3.3.4 Determining the Order of the State Equations.....	27
3.4 Orbital Parameters.....	31
3.5 Parameters for Data Generation.....	32
3.6 Experimental Procedure.....	33
3.7 Equipment.....	34
3.8 Summary.....	34
IV. Results and Analysis.....	35
4.1 Introduction	35
4.2 Estimator Performance Using Perfect Data.....	35
4.2.1 Low Orbit.....	36
4.2.2 High Orbit	44
4.3 Estimator Performance Using Noisy Data.....	52
4.3.1 Residuals	52
4.3.2 Accuracy of Estimate	59
4.3.3 Covariance Matrix.....	63
4.4 Summary.....	64

	Page
V. Conclusions and Recommendations	65
5.1 Introduction	65
5.2 Conclusions.....	65
5.3 Recommendations	66
5.4 Potential Areas of Study	67
5.5 Summary.....	68
Appendix A. Coordinate Frame Transformations.....	69
A.1 Determining LMST and Site ECI Coordinates.....	69
A.2 Earth Centered Inertial (ECI) to Topocentric Transformation	71
A.3 Topocentric to ECI Transformation	72
Appendix B. The Data Linearization Matrix, H	73
Appendix C. State Transition Matrix, Φ	75
C.1 The Two-body Terms.....	75
C.2 The J2 Terms.....	77
Bibliography	80
Vita	81

List of Figures

Figure	Page
1. Gaussian Distribution	7
2. Position and velocity components in ECI coordinates	18
3. Coordinates for Geopotential.....	19
4. Position Error vs. Timestep for eom4, eom4a, and eom4b	29
5. Position Error vs. Timestep for eom4a and eom4b.....	30
6. Plot of Pass Duration vs. Max Elevation.....	32
7. Converged RMS Residuals vs. Track Length -- Low Orbit	38
8. Converged Mean Residuals vs. Track Length -- Low Orbit	39
9. Converged RMS Residuals vs. Max Elevation -- Low Orbit	40
10. Converged Mean Residuals vs. Max Elevation -- Low Orbit.....	41
11. Position and Velocity Errors vs. Track Length -- Low Orbit.....	42
12. Position and Velocity Errors vs. Max Elevation -- Low Orbit	43
13. Converged RMS Residuals vs. Track Length -- High Orbit	46
14. Converged Mean Residuals vs. Track Length -- High Orbit.....	47
15. Converged RMS Residuals vs. Max Elevation -- High Orbit.....	48
16. Converged Mean Residuals vs. Max Elevation -- High Orbit.....	49
17. Position and Velocity Errors vs. Track Length -- High Orbit.....	50
18. Position and Velocity Errors vs. Max Elevation -- High Orbit	51
19. Average Mean and RMS Residuals After Convergence versus Max Elevation	54
20. Average RMS Residuals Before and After Correction versus Max Elevation	55
21. Residual Values Before and After Correction - Low El Pass	56
22. Residual Values Before and After Correction - High El Pass	57

Figure	Page
23. Residual Values versus One Sigma After Convergence - Low El Pass	58
24. Position and Velocity Errors versus Max Elevation - Low Orbit	60
25. Position and Velocity Errors versus Max Elevation - High Orbit	61
26. Position and Velocity Errors versus Max Elevation - High Data Rate	62
27. Relationship between Mean Equinox, GMST, and LMST (8: 23)	69
28. Geocentric and geodetic latitude (2: 95)	70

List of Tabless

Table	Page
1. Reference Orbits for Truth Model Validation	21
2. Highest Order of Approximation in Equations of State.....	21
3. Test Orbits for Estimator Validation	27
4. Position and Velocity Errors from 3rd and 4th Order Taylor Series.....	28
5. Effective Time Duration for State Equations	30
6. Orbital Elements - Satellite 20003	31
7. Orbital Elements - Satellite 20004	31
8. Schedule of Passes for Data Collection.....	33
9. Position and Velocity Errors from Perfect Data -- Low Orbit.....	37
10. Position and Velocity Errors from Perfect Data -- High Orbit.....	45
11. Comparison of Predicted and Actual Estimator Accuracy.....	63

Abstract

This study investigated the use of a least squares differential corrector to compress the information contained in a single radar track of a Near Earth satellite into a six element, Earth Centered Inertial state vector and associated covariance matrix. Observations were generated using a truth model program based on two-body, J_2 geopotential, and atmospheric drag dynamics and consisted of simulated range, azimuth and elevation. Random Gaussian noise was added to the data to simulate the random errors seen in real world observations. The orbital dynamics used in the estimator consisted of two-body and J_2 geopotential effects which were approximated using a Taylor Series expansion in time. Analysis was conducted using two circular, inclined low earth orbits. Estimator performance was evaluated as a function of maximum pass elevation, track duration, data rate and the highest order of approximation of the equations of state. The estimator successfully extracted all of the pertinent information from the data with accuracy being dependent on the number of data points available. A correlation between the required order of approximation and maximum expected track length was also noted.

COMPRESSION OF A RADAR TRACK OF A NEAR EARTH SATELLITE INTO AN EARTH CENTERED INERTIAL STATE VECTOR USING LEAST SQUARES DIFFERENTIAL CORRECTION

I. Background and Statement of the Problem

1.1 Introduction

The Space Surveillance Center (SSC), located in Cheyenne Mountain Air Force Base, Colorado, is the world's premier space tracking organization. Through the use of a world wide network of ground based radars and electro-optical cameras known as the Space Surveillance Network (SSN), the SSC tracks and maintains orbital predictions for all man-made objects in orbit about the earth with a radar cross section of at least ten square centimeters. Satellites with a period less than 225 minutes are defined as *Near Earth* satellites. Almost all of the data used to track near earth satellites comes from ground based space surveillance and ballistic missile early warning (BMEWS) radars.

When these radars track a satellite they produce data called *observations* which are sent to the SSC over a telecommunication link. In their most basic form this data consists of the time, elevation, azimuth and range of the satellite as observed from the site. A typical track for a near earth object might span from five to twenty-five minutes. Since some of these radars can measure the position of a satellite as fast as 100 times each second, this could result in 30,000 to 150,000 observations per track (7: 156). Obviously, transmitting this much data to the SSC every time a satellite is tracked is not feasible. Instead, the radar sends only a representative sampling of this data to the SSC. Typically, this consists of three observations positioned at the beginning, middle and end of the track. For very low priority satellites perhaps only one observation will be sent to the SSC.

The SSC combines this new data along with observations from other sensors using batch and/or sequential processing to update the satellite's orbital elements or *elset*. Every catalogued satellite still in orbit has its own elset which is continuously maintained using the observations sent in by the SSN. These elsets are then used to predict satellite positions in the near future using both general and special perturbation methods. One important use for these updated elsets is to allow sensors to acquire and track satellites. Maintaining an accurate and timely database is also important in avoiding satellite collisions and providing warning of over flights of foreign intelligence satellites.

With over 7,000 objects in orbit and more than twenty six sensor sites in the SSN, the SSC typically receives 50,000 to 80,000 observations per day. This is a large amount of data to be transmitted to and processed by the SSC computer. As space continues to increase in importance for both military and commercial purposes, the number of objects in earth orbit will increase. This will result in additional work loads for both the sensors making up the SSN, for the SSC computer and personnel, and for the communications links that tie them together.

If a way could be found to more efficiently use the information gathered by the sensors in the SSN it might be possible to alleviate some of the heavy demands that can be expected. This would allow existing resources to handle the job without expensive investments to upgrade facilities and equipment. One way to do this would be to compress all of the data into a single state vector and associated covariance matrix. This would allow all of the information contained in the track to be sent to the SSC instead of a very small sample. Not only would this provide the SSC with better data which could reduce the frequency of required updates or sensor tasking, but it distributes some of the processing load out to the sensor sites.

1.2 Problem Statement

In order to increase the capacity of the SSC and SSN to track and maintain elsets on the growing population of near earth space objects, it is necessary to develop a method of compressing all of the information contained in a sensor track into an easily transmitted and utilized form. The method must be easily implemented and not require significant equipment upgrades. A possible solution is to have each

sensor site convert all of its observations into a state vector and associated covariance matrix using a least squares batch differential correction based on two-body dynamics and possibly J_2 effects.

1.3 Research Objectives

The first objective is to develop a truth model to generate simulated ground sensor site observations. The truth model should model satellite motion using two-body orbital dynamics, the J_2 zonal harmonic, and air drag since these are the three dominant factors in the orbital motion of near earth satellites. Output from the truth model will consist of accurate time, range, azimuth, and elevation values to which Gaussian random noise will be added to simulate real world observations.

The second objective is to create a differential corrector based on least squares estimation operating in a batch mode. The dynamics model used in the estimator will be based on a Taylor Series expansion of the equations of motion for an object in orbit about the earth. The state transition matrix used in the estimator will be derived from these same Taylor Series equations.

The third objective is to investigate the effectiveness of the differential corrector in reducing the simulated observations from the truth model into a single state vector and associated covariance matrix. Specifically, it will be necessary to determine how many terms are needed in the Taylor Series approximation of the equations of motion. Also it must be determined if the equations of motion must include the J_2 zonal harmonics or if the two-body dynamics alone are sufficient. And finally, the correlation between pass time (or maximum elevation) and the effectiveness of the estimator will be studied.

1.4 Research Questions

Least squares estimation is a commonly used method for performing differential correction on the orbital elements or state of satellites. It is especially effective when used in a batch mode where sufficient observations exist to span a significant portion of the object's orbit. In the case of a single track by a ground based sensor site of a near earth satellite, only a small part of the orbit will be observed. Two factors that will influence the number of observations will be the objects maximum elevation relative to the site and its altitude.

This leads to the following questions:

1. Does it matter how good the dynamics model used by the estimator is?
 - a. Are the effects of the J_2 zonal harmonic or of atmospheric drag large enough to be significant?
 - b. How many terms must be included in the Taylor Series expansion of the equations of state?
2. What is the minimum number of observations required by the estimator to effectively compress the data into a single state vector and covariance matrix?
3. Can this be related to the maximum elevation of the pass and/or the satellites altitude during the pass? If so, what is this relationship?

1.5 Assumptions

Although there exist numerous perturbation sources, only those perturbations caused by the J_2 zonal effect and atmospheric drag are considered in the truth model. This is based on the reasonable assumption that the other perturbations are too small to be noticeable -- especially during the short track times for near earth objects.

Normally, several days worth of data are required to estimate the effect of drag on an orbit. The SSC typically uses observations spaced over a period of 3-7 days to determine the drag experienced by a Near Earth satellite. Because this study looks at reducing the data from a single track, insufficient data is available for estimating the effect of drag. Therefore the estimator will use only two-body and J_2 effects.

The truth model generates accurate ephemeris information for the input satellite reference trajectory. The data is assumed to be perfect and is made more realistic by applying Gaussian random noise to the data.

There are errors associated with the dynamics, the state vector, and the observations. The estimation routines developed during this study assume that the use of a Taylor Series expansion will result in a dynamics model that is *close enough* to reality and that the major source of uncertainty comes from the observations.

1.6 Scope

The proposed study models the effectiveness in applying a two-body least squares batch estimator to a short arc of observations to create a single state vector and associated covariance matrix. The main efforts in this thesis are: (1) developing a truth model to generate simulated observations from ground based sensor sites, (2) building a least squares differential corrector to generate an earth centered inertial (ECI) state vector and covariance matrix, and (3) analyzing the effectiveness of this estimator in reducing or *compressing* the data for near earth satellite passes.

1.7 Summary

As the number of objects in earth orbit continues to increase along with the growing importance of space in general, the demands made on the SSC and SSN to track and predict the motion of these objects will also increase. Instead of spending large sums of money to upgrade facilities and equipment it may be possible to multiply the effectiveness of current capabilities of the SSC and SSN.

One possible solution is to compress all of the information from a single sensor track so that it can be easily transmitted to and used by the SSC. This could be done by using a least squares batch differential corrector to reduce the data obtained at the sensor site into a single state vector and associated confidence (covariance) matrix. This would essentially extract more usable data from each sensor track. It is hoped that this would allow for more accurate elsets to be maintained at the SSC. This in turn could reduce the frequency with which elsets must be updated and would essentially preprocess the observations, thus reducing the computational load on the SSC computer. Additionally, it might be possible to reduce the number of tracks or the fraction of a track required on each satellite, thereby allowing the SSN to track more objects with existing or reduced resources.

II. Theoretical Background

2.1 Introduction

For almost as long as man has been on earth, he has looked up into the night sky and wondered about the things he saw there. As far back as 3000 B.C., Babylonian priest-astrologers were observing and recording the motions of the moon, sun and the five visible planets. As time passed, ancient man attempted to devise explanations for how the planets moved but it was not until the early 1600's that Kepler finally developed his three laws which correctly described the motion of these heavenly bodies. However, Kepler's explanation merely stated how the planets (or any other object in space for that matter) moved — it did not answer the more fundamental question of why. Although Galileo had a few ideas, it was Isaac Newton who finally answered the question when he published his three laws of motion and the law of universal gravitation (1:757-758).

The first method for finding the orbit of an object from observations was published by Newton in the *Principia*. This method required three observations (angles only since radars did not exist in 1705) and consisted of a graphical approach using successive approximations. The first analytical method for solving this same problem was presented by Euler in his *Theory of the Motion of Planets and Comets* in 1744. Euler also developed a relationship which related any two position vectors with the vector connecting them and the time interval between the two vectors. Further refinements to Euler's work were produced by Lambert and Lagrange but it was not until Laplace developed a new method in 1780 that it was possible to process more than three observations at a time (2:51-53, 117-122). By 1802, Karl Frederick Gauss had developed yet another method for using three observations to determine the orbital elements of an object, the basic elements of which are still used today.

As important as all these developments were, an even more important contribution to the science of orbit determination was Gauss' method of least squares. By using the method of least squares it was possible to use more than three observations to determine the orbit of an object to far greater precision

than before by producing orbital elements that agreed with all of the observations used rather than with just two or three. As Gauss himself wrote:

Finally, as all our observations, on account of the imperfection of the instruments and of the senses, are only approximations to the truth, an orbit based only on the six absolutely necessary data may still be liable to considerable errors. In order to diminish these as much as possible, and thus to reach the greatest precision attainable, no other method will be given except to accumulate the greatest number of the most perfect observations, and to adjust the elements, not so as to satisfy this or that set of observations with absolute exactness, but so as to agree with all in the best possible manner. (3)

2.2 The Method of Least Squares

The fundamental elements of least squares are built on four basic assumptions: that the dynamics contain no error, that the observations do contain errors, that the observational errors obey a Gaussian distribution, and that the *Principle of Maximum Likelihood* applies. The last item comes from Gauss' groundbreaking work in the field of probability theory and states that the value of an estimate which maximizes the probability of obtaining a particular set of data is the true value (4: 22). The third assumption is supported by the *Central Limit Theorem*, also developed by Gauss, which states that the errors in the observation data will follow a normal distribution (see Figure 1) as long as the total error is the product of many small error sources (4: 11).

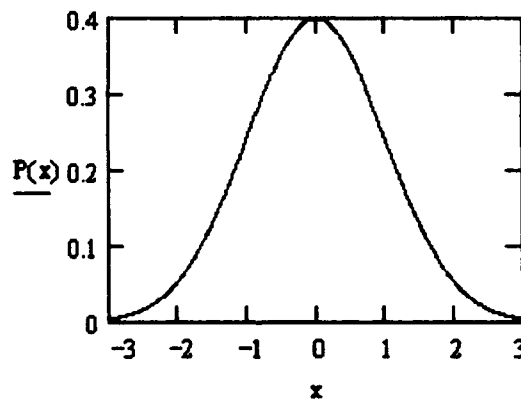


Figure 1. Gaussian Distribution

The assumption that the errors associated with the observation data follow a normal or Gaussian distribution is a key element in the development of estimation theory. Therefore the probability of an error is governed by the *Gaussian probability density function*:

$$P(e)de = \frac{1}{\sigma\sqrt{2\pi}} \exp\left(\frac{-e^2}{2\sigma^2}\right)de \quad (1)$$

where $P(e)$ is the probability that an error e will occur. This implies that the probability of an error is defined by the area under the curve containing the error in question. Thus it is necessary to define a range of errors, such as e and $e + \delta e$, in order to calculate the probability. Eq (1) and Figure 1 demonstrate several important features of a Gaussian distribution: (1) The distribution is symmetric about the true value of the measurement. (2) The width of the curve is determined by the *standard deviation* σ . (3) The total area under the curve is one because the function is normalized. This means that there will always be some error in a measurement, although small errors are more likely than large ones. A large value of σ results in a broad curve, signifying low precision, while a small value of σ results in a narrow curve, signifying high precision.

The next step in the development of estimation theory involves the estimation operator:

$$E(-) \equiv \int_{-\infty}^{\infty} (-) f(x) dx \quad (2)$$

where the open slot $(-)$ contains the quantity to be estimated and $f(x)$ is a probability density function. By applying the estimation operator three special results are obtained: (1) The expected value of a measurement is the true value: $E(x) = x_0$. (2) The average error in the measurement is zero: $E(e = x - x_0) = 0$. (3) The average squared error is σ^2 : $E(e^2) = \sigma^2$ (4:19-20).

For the case where only a single value is to be estimated, such as the length of a rod, the probability of obtaining a particular set of *independent* measurements is given by:

$$P(x_1, x_2, \dots, x_N) = (2\pi)^{-N/2} \left[\prod_{i=1}^N \sigma_i^{-1} \right] \exp\left(-\sum_{i=1}^N \frac{(x_i - x_0)^2}{2\sigma_i^2}\right) \quad (3)$$

where σ_i is the standard deviation associated with each measurement, N is the total number of measurements, x_i is the value of each measurement, and x_o is the true value. Since the true value can never be known, it is necessary to apply the Principle of Maximum Likelihood which allows the replacement of x_o with its estimate \bar{x} (4:22). In order to maximize the probability of the data with respect to the estimate, the argument of the exponential must be minimized:

$$\frac{d}{d\bar{x}} \sum_{i=1}^N \frac{(x_i - \bar{x})^2}{2\sigma_i^2} = 0 \quad (4)$$

giving

$$\sum_{i=1}^N \frac{(x_i - \bar{x})}{\sigma_i^2} = 0 \quad (5)$$

It is from Eq (4) that this estimation method derives its name of least squares. The quantity $(x_i - \bar{x})$ is usually called the *residual*, r_i , which can be thought of as an estimate of the true error. Solving for the estimate \bar{x} gives:

$$\bar{x} = \frac{\sum_{i=1}^N x_i / \sigma_i^2}{\sum_{i=1}^N 1 / \sigma_i^2} \quad (6)$$

2.3 Multi-Dimensional Least Squares

The preceding section showed the development of least squares estimation theory for a one dimensional or single variable case. However, most problems (such as orbit estimation) are multi-dimensional in nature. Fortunately, the results from section 2.3 can be extended to support multi-dimensional problems. To start, define the following notation:

$$\mathbf{x}^T = (x_1, x_2, x_3, \dots, x_N) \quad (7)$$

and

$$\mathbf{P} = \begin{pmatrix} \sigma_{11}^2 & \sigma_{12}^2 & \dots & \sigma_{1N}^2 \\ \sigma_{21}^2 & \sigma_{22}^2 & \dots & \sigma_{2N}^2 \\ \dots & \dots & \dots & \dots \\ \sigma_{N1}^2 & \sigma_{N2}^2 & \dots & \sigma_{NN}^2 \end{pmatrix} \quad (8)$$

where \mathbf{x}^T is the *state* or variables in the problem and \mathbf{P} is the *covariance matrix*. The covariance matrix contains information on the variance associated with each element in the state vector. The diagonal entries are called variances while the off-diagonal entries are referred to as covariances. Using this notation the Gaussian probability density function can be written as:

$$f(\mathbf{x}) = (2\pi)^{-N/2} |\mathbf{P}|^{-1/2} \exp\left(-\frac{1}{2}(\mathbf{x} - \mathbf{x}_0)^T \mathbf{P}^{-1}(\mathbf{x} - \mathbf{x}_0)\right) \quad (9)$$

where the variable $\bar{\mathbf{x}}$ has been replaced by the estimated state $\bar{\mathbf{x}}$, and the standard deviation squared, σ^2 , has been replaced by the covariance matrix \mathbf{P} . As before, the argument of the exponential is the quantity to be minimized, yielding:

$$(\mathbf{x} - \mathbf{x}_0)^T \mathbf{P}^{-1}(\mathbf{x} - \mathbf{x}_0) \geq 0 \quad (10)$$

which means the covariance matrix \mathbf{P} must be a *positive semi-definite matrix* (4:27).

2.4 Linearizing the Problem

The problem of orbit determination is fundamentally a nonlinear one. Not only are the dynamics highly nonlinear but so is the relationship between observations and the satellite's state. However, in order to make any progress in estimating the state of a satellite it is necessary to linearize various aspects of the problem.

To start, the dynamics must be specified, either as a set of differential equations

$$\frac{d\mathbf{x}}{dt} = f(\mathbf{x}, t) \quad (11)$$

or as an explicit solution

$$\mathbf{x}(t) = \mathbf{h}(\mathbf{x}(t_0), t) \quad (12)$$

which gives the state as a function of time and the initial conditions. Since the dynamics are deterministic, these equations can be linearized as:

$$\delta\mathbf{x}(t) = \Phi(t, t_0)\delta\mathbf{x}(t_0) \quad (13)$$

where $\Phi(t, t_0)$ is the *state transition matrix* relating a change in the state at time t to a change in the initial conditions at time t_0 . If the dynamics are given explicitly as a function of time then the state transition matrix is given by:

$$\Phi(t, t_0) = \nabla_{\mathbf{x}(t_0)} \mathbf{h}(\mathbf{x}(t_0), t) \quad (14)$$

As was pointed out earlier, the true state \mathbf{x}_0 will always be unknown and since the whole purpose of least squares is to produce an estimate $\bar{\mathbf{x}}$, a *reference state* \mathbf{x}_{ref} must be specified about which the dynamics can be linearized. The relationship between the reference state and the estimate is:

$$\bar{\mathbf{x}} = \mathbf{x}_{\text{ref}} + \delta\mathbf{x} \quad (15)$$

where $\delta\mathbf{x}$ is the correction needed to turn the reference state into the estimate. Hopefully the initial guess of the state will be close enough to the true state to allow the linearized dynamics to be valid. By making successive corrections to the reference state, it should be possible to converge to the correct estimate of the true state.

The relationship between the observations and the system state can be written as

$$\mathbf{z}_i(t_i) = \mathbf{G}(\mathbf{x}(t_i), t_i) + \mathbf{e}_i \quad (16)$$

where \mathbf{z}_i is the observation vector, such as {range, azimuth, elevation}, \mathbf{G} is the function which converts the state variables at time t_i to the observation variables, and \mathbf{e}_i is the true error associated with the observation. Since this relationship is also usually nonlinear it will be necessary to linearize it as well:

$$\begin{aligned}
\mathbf{e} &= \mathbf{z} - \mathbf{z}_0 \\
&= \mathbf{G}(\mathbf{x}, t) - \mathbf{G}(\mathbf{x}_0, t) \\
&= \mathbf{G}(\mathbf{x}_0 + \delta\mathbf{x}, t) - \mathbf{G}(\mathbf{x}_0, t) \\
&\approx \frac{\partial \mathbf{G}}{\partial \mathbf{x}} \delta\mathbf{x}(t)
\end{aligned} \tag{17}$$

where \mathbf{z} is the actual observation vector, \mathbf{z}_0 is the observation vector using perfect data, \mathbf{x} is the observed state, \mathbf{x}_0 is the true state, and $\delta\mathbf{x}$ is the difference between the true and observed states. Replacing \mathbf{x} in Eqs (16) and (17) with \mathbf{x}_{ref} allows the definition:

$$\mathbf{H}_i(t_i) \equiv \frac{\partial \mathbf{G}}{\partial \mathbf{x}}(\mathbf{x}_{ref}(t_i), t_i) \tag{18}$$

which relates the error in the state to the error in the reference trajectory (4:69).

2.5 Correcting the Reference State

Just as before, the concept of finding the residual instead of the true error must be used

$$\mathbf{r}_i = \mathbf{z}_i - \mathbf{G}(\mathbf{x}_{ref}(t_i), t_i) \tag{19}$$

where the residual vector \mathbf{r} is formed from the observed location \mathbf{z} minus the predicted location $\mathbf{G}(\mathbf{x})$. If the reference state is close enough to the true state, then the residual vector will be linearly related to changes in the reference state (4:70):

$$\begin{aligned}
\delta\mathbf{r}_i &\approx \mathbf{H}_i \delta\mathbf{x}(t_i) = \mathbf{H}_i \Phi(t, t_0) \delta\mathbf{x}(t_0) \\
&= \mathbf{T}_i \delta\mathbf{x}(t_0)
\end{aligned} \tag{20}$$

and

$$\mathbf{r}'_i \approx \mathbf{r}_i + \delta\mathbf{r}_i = \mathbf{r}_i - \mathbf{T}_i \delta\mathbf{x}(t_0) \tag{21}$$

where \mathbf{r}' is the residual vector after the reference state is corrected to be the estimate, and \mathbf{r}_i is the residual vector associated with the reference state. The matrix \mathbf{T} is called the observation matrix and is defined as

$$\mathbf{T}_i \equiv \mathbf{H}_i \Phi(t_i, t_0) \quad (22)$$

Since least squares is normally used with multiple observations it will be convenient for notation purposes to define three items. The first is the total residual vector

$$\mathbf{r}^T \equiv [\mathbf{r}_1^T \quad \mathbf{r}_2^T \quad \dots \quad \mathbf{r}_N^T] \quad (23)$$

where each \mathbf{r}_i is itself a vector of residuals. The second is the observation matrix

$$\mathbf{T} \equiv \begin{bmatrix} \mathbf{T}_1 \\ \mathbf{T}_2 \\ \dots \\ \mathbf{T}_N \end{bmatrix} = \begin{bmatrix} \mathbf{H}_1 \Phi(t_1, t_0) \\ \mathbf{H}_2 \Phi(t_1, t_0) \\ \dots \\ \mathbf{H}_N \Phi(t_1, t_0) \end{bmatrix} \quad (24)$$

The third is the total instrumental covariance matrix in block-diagonal form

$$\mathbf{Q} \equiv \begin{bmatrix} \mathbf{Q}_1 & 0 & \dots & 0 \\ 0 & \mathbf{Q}_2 & \dots & 0 \\ \dots & \dots & \dots & \dots \\ 0 & 0 & \dots & \mathbf{Q}_N \end{bmatrix} \quad (25)$$

where each \mathbf{Q}_i is itself a matrix of the instrumental covariance associated with each data vector \mathbf{z}_i . In the form shown, each data vector is statistically independent and therefore the off-diagonal entries are zero.

In accordance with the Principle of Maximum Likelihood, the estimate $\bar{\mathbf{x}}$ is the value of the state which maximizes the probability $P(\mathbf{r})$. Since the error statistics are assumed to be Gaussian

$$P(\mathbf{r}) = (2\pi)^{-N/2} |\mathbf{Q}|^{-1/2} \exp\left(-\frac{1}{2} \mathbf{r}^T \mathbf{Q}^{-1} \mathbf{r}\right) \quad (26)$$

where the residual vector \mathbf{r} is the residual vector associated with the estimate $\bar{\mathbf{x}}$. Substituting Eq (21) into Eq (26) leads to the minimization of

$$\frac{\partial}{\partial \mathbf{x}} \left[(\mathbf{r} - \mathbf{T}\delta\mathbf{x})^T \mathbf{Q}^{-1} (\mathbf{r} - \mathbf{T}\delta\mathbf{x}) \right] = 0 \quad (27)$$

where \mathbf{r} is the total residual vector associated with the reference state \mathbf{x}_{ref} . From here it is possible to solve for the correction, new estimate and associated covariance matrix as

$$\delta\mathbf{x}(t_0) = (\mathbf{T}^T \mathbf{Q}^{-1} \mathbf{T})^{-1} \mathbf{T}^T \mathbf{Q}^{-1} \mathbf{r} \quad (28)$$

$$\bar{\mathbf{x}}(t_0) = \mathbf{x}_{\text{ref}}(t_0) + \delta\mathbf{x}(t_0) \quad (29)$$

$$\begin{aligned} \mathbf{P}_{\delta\mathbf{x}} &= E(\mathbf{r}_{\delta\mathbf{x}} \mathbf{r}_{\delta\mathbf{x}}^T) \\ \mathbf{P}_{\bar{\mathbf{x}}} &= (\mathbf{T}^T \mathbf{Q}^{-1} \mathbf{T})^{-1} \end{aligned} \quad (30)$$

where \mathbf{T} , \mathbf{Q} , and \mathbf{r} are the total matrices and vector defined earlier (4:60-63,70).

It is important to note that the estimate found in Eq (29) is the correct answer only if the reference has *converged* to a solution. In general, the estimate becomes a new reference state and the whole process is repeated until convergence is attained. One practical convergence standard is for successive values of $\delta\mathbf{x}$ to be within the one σ values provided by $\mathbf{P}_{\delta\mathbf{x}}$ and for the residuals to also agree with their expected σ values (4: 77).

2.6 Implementing Least Squares on a Computer

When working with large amounts of data, the matrix and vector equations introduced above can become large and unwieldy. For this reason, it is usual to process the data one observation at a time using the following running sums:

$$\mathbf{A} = \sum_i \mathbf{T}_i^T \mathbf{Q}_i^{-1} \mathbf{T}_i \quad (31)$$

$$\mathbf{B} = \sum_i \mathbf{T}_i^T \mathbf{Q}_i^{-1} \mathbf{r}_i \quad (32)$$

After all of the data is processed the correction to the state and the covariance matrix can be found from

$$\begin{aligned} \mathbf{P}_{\delta\mathbf{x}} &= \mathbf{A}^{-1} \\ \delta\mathbf{x}(t_0) &= \mathbf{P}_{\delta\mathbf{x}} \mathbf{B} \end{aligned} \tag{33}$$

where $\delta\mathbf{x}$ is the correction that turns the reference state into either the estimate or a better reference state and $\mathbf{P}_{\delta\mathbf{x}}$ is the covariance matrix associated with the corrected state (4:64,72).

2.7 Summary

The method of least squares is a proven approach to estimating the state of a satellite from a large number of observations. When used in a differential corrector it allows for the iterative correction of an initial reference state to the correct estimate of the true state. It does this by adjusting the reference state to produce a trajectory that agrees best (i.e. minimizes the squared error) with all of the data instead of agreeing perfectly with only two or three observations. Least squares also has the property that the accuracy of the estimate increases as the number of data points increases although the relationship is not linear. For example, if only one variable is involved it can be shown that:

$$\sigma_{\bar{x}} = \frac{\sigma_i}{\sqrt{N}}$$

where $\sigma_{\bar{x}}$ is the standard deviation of the estimate, N is the number of data points, and σ_i is the standard deviation of each measurement (a constant in this case).

III. Methodology

3.1 Introduction

The data used in this research was produced using a two-step procedure in which simulated observation data was converted into a state vector and associated covariance matrix. The first step involved the use of a truth model to generate simulated range, azimuth, and elevation observations for a single track of a satellite as seen by a space surveillance radar located on the surface of the earth. In the second step, this track of data was reduced to a state vector and covariance matrix using least squares differential correction. Error statistics were also generated and the accuracy of the estimated state was calculated by comparing it to the true state.

Analysis of the data concentrated on evaluating how good the estimator was in concentrating all of the data available in the track into the estimated state vector. The effects of different dynamics models, data acquisition rate, and maximum elevation of the pass were investigated using the error statistics and accuracy of each estimate.

3.2 The Truth Model

The truth model simulates the orbital motion of a satellite by using two-body dynamics plus J_2 zonal harmonic and atmospheric drag perturbations. Because this study concentrates on relatively short arcs (22 minutes or less) of near earth orbits, it was felt that other perturbations such as the higher order geopotential terms and n-body effects were insignificant and could be ignored.

3.2.1 Program Execution. Input to the truth model consists of an initial state containing position and velocity (expressed in ECI coordinates), an epoch (or start) time, the end time for the arc in question, and the time step between each data point. The program then numerically integrates the equations of motion using a fourth order Hamming predictor-corrector routine. The predictor part is based on a fourth-order Milne method predictor and the corrector method is derived from fourth-order Milne and Adams-Moulton predictor-corrector methods (5:391). Since this method requires four previous values of the state in order

to predict the next value, a Picard iteration is used to generate three future state values based on the initial state (6:108-109).

Output generated by the program consists of ephemerides and observations which are written to two separate files for later use by the estimator programs. After each ephemeris point is generated a subroutine is called to convert the ECI position of the satellite into topocentric observations relative to an imaginary sensor site located in the Indian Ocean (see Appendix A). If the elevation of this "observation" is greater than zero then it is assumed that the sensor can see the satellite and so the ephemeride and its associated observation are written to their respective data files. If the elevation is less than zero, then the output data files are not modified and the next position calculated. This basic cycle is repeated until the specified end time has been reached.

In order to better model the real world, the observations are modified by the addition of simulated errors or noise. This is done using a Gaussian pseudo-random number generator and assumed values for the one-sigma accuracy of the radar in range, azimuth, and elevation. For purposes of this study the assumed values were: 100 meters in range, 0.025 degrees in azimuth, and 0.025 degrees in elevation. Since a new seed value is used every time the number generator is called, each value output will be different and the overall distribution will be very close to the normal distribution shown in Figure 1. Multiplying the one-sigma values by the random numbers results in the simulated errors also following a Gaussian distribution.

Several special options were built into the truth model program to facilitate the testing and research objectives. The program allows for the time step to be changed from within the program. This meant that the input file did not have to be edited for the single purpose of changing the time step. Also, the addition of noise or drag perturbations could be turned off prior to starting the numerical integration. Turning off the noise permits the generation of "perfect" data for testing purposes, while turning off the drag allows for investigation of the significance of drag in affecting the estimate and covariance matrix.

3.2.2 *The Equations of Motion.* The baseline for the equations of motion is the first order differential equations from the solution of the two-body problem. In vector notation, the two-body equation of motion is:

$$\ddot{\mathbf{r}} + \frac{\mu}{r^3} \mathbf{r} = 0 \quad (34)$$

where the vector \mathbf{r} extends from the earth's center of mass to the satellite's center of mass, r is the magnitude of this vector and μ is the *gravitational parameter* of the earth and is defined as $\mu = GM$, where G is the universal gravitational constant and M is the mass of the earth. In a rectangular coordinate system (such as ECI), Eq (34) leads to six first order differential equations:

$$r = \sqrt{x^2 + y^2 + z^2} \quad (35)$$

$$\begin{aligned} \dot{x} &= u \\ \dot{y} &= v \\ \dot{z} &= w \end{aligned} \quad (36)$$

$$\begin{aligned} \dot{u} &= -\mu x / r^3 \\ \dot{v} &= -\mu y / r^3 \\ \dot{w} &= -\mu z / r^3 \end{aligned} \quad (37)$$

where x, y, z are the components of the position vector, and u, v, w are the components of the velocity vector (reference Figure 2).

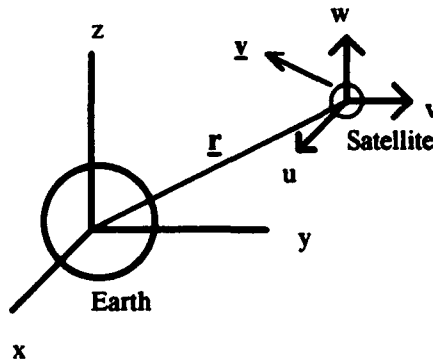


Figure 2. Position and velocity components in ECI coordinates.

The most significant of the various geopotential effects is found in the second zonal harmonic, usually referred to as the J_2 geopotential term or simply the J_2 term, which is caused by the earth's oblateness (6:59,80). This term is normally written in spherical coordinates as:

$$V_{20} = \frac{\mu R_e^2 J_2}{2r^3} (3 \cos^2 \theta - 1) \quad (38)$$

where R_e is the earth's equatorial radius, J_2 is the coefficient for the second zonal harmonic, and θ is the angle between the Z coordinate axis and the satellites position vector (reference Figure 3) (6:59). In order to convert this geopotential term to ECI coordinates it is necessary to rewrite the angle as $\cos \theta = z/r$. If the constants on the right side of Eq (38) are collected as:

$$A = \frac{1}{2} \mu R_e^2 J_2 \quad (39)$$

then Eq (38) can be rewritten in cartesian coordinates as:

$$V_{20} = A \left(3 \frac{z^2}{r^5} - \frac{1}{r^3} \right) \quad (40)$$

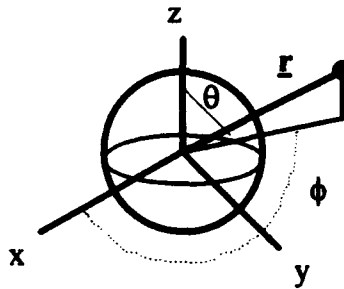


Figure 3. Coordinates for Geopotential

The effect of the geopotential manifests itself as an additional acceleration of the satellite which is related to the geopotential through the gradient operator:

$$\mathbf{a}_{20} = -\nabla V_{20}(x, y, z) \quad (41)$$

where a_{20} is the additional acceleration due to the J_2 geopotential term. Calculating the gradient results in an additional term for each of the velocity-dot equations:

$$\begin{aligned} \mathbf{a} &= \mathbf{a}_{2body} + \mathbf{a}_{20} \\ \begin{pmatrix} \dot{u} \\ \dot{v} \\ \dot{w} \end{pmatrix} &= -\frac{\mu}{r^3} \begin{pmatrix} x \\ y \\ z \end{pmatrix} - A \begin{pmatrix} 3x/r^5 - 15xz^2/r^7 \\ 3y/r^5 - 15yz^2/r^7 \\ 9z/r^5 - 15z^3/r^7 \end{pmatrix} \end{aligned} \quad (42)$$

The basic equation for modeling the effect of atmospheric drag is:

$$\begin{aligned} \mathbf{a}_d &= -\frac{1}{2} C_D \frac{A}{m} \rho V_a \dot{\mathbf{r}}_a \\ V_a &= |\dot{\mathbf{r}}_a| = \left| \left\{ \dot{x} + \dot{\theta}y, \dot{y} - \dot{\theta}x, \dot{z} \right\} \right| \end{aligned} \quad (43)$$

where \mathbf{a}_d is the effect of air drag, C_D is the satellite's coefficient of drag, A/m is the satellite's ratio of cross sectional area to mass, ρ is the atmospheric density, $\dot{\mathbf{r}}_a$ is the satellite's velocity relative to the atmosphere, and $\dot{\theta}$ is the rotational rate of the earth (atmosphere is assumed to rotate with the earth) (2:423-424). The quantity $C_D A/m$ is often lumped together and called B^* . For the purposes of this study, the satellite was assumed to have a $C_D = 2.0$, $A = 7.5 \text{ m}^2$, and $m = 1000 \text{ kg}$.

The atmospheric density was modeled using the 1976 Standard Atmosphere in which the density, as a function of height, is given by:

$$\rho(h) = \exp \left[-\left(\frac{z_1}{h}\right)^4 + \left(\frac{z_2}{h}\right)^3 - \left(\frac{z_3}{h}\right)^2 + \left(\frac{z_4}{h}\right) - \left(\frac{h}{z_5}\right)^4 + \left(\frac{h}{z_6}\right)^3 - \left(\frac{h}{z_7}\right)^2 + \left(\frac{h}{z_8}\right) - z_9 \right]$$

where $\rho(h)$ is in kg-m^{-3} , h is the altitude in kilometers and

$$\begin{aligned} z_1 &= 246482.873 & z_2 &= 5377132.030 & z_3 &= 1536228.60 & z_4 &= 19174788.0 & z_5 &= 105.381650 \\ z_6 &= 4968.56120 & z_7 &= 56060.0780 & z_8 &= 160314.760 & z_9 &= 344944.780 \end{aligned}$$

This model is valid for altitudes between 100-1000 km (8).

3.2.3 Program Validation. Proper operation of the truth model was validated by incrementally testing its accuracy using three models of the dynamics: (1) two-body only, (2) two-body plus J_2 , and (3) two-body plus J_2 plus drag. The two-body test was done using a circular reference orbit which allowed for easy calculation of the satellites position as a function of time. To test the J_2 part, two different reference orbits were used (see Table 1).

Table 1. Reference Orbits for Truth Model Validation

Inclination (deg)	Eccentricity	Period (min)	Apogee Ht (km)	Perigee Ht (km)	Nodal Regression	Apsidal Rotation
7.33	0.0166	91.19	444.4	221.6	8.3 deg/day	17.8 deg/day
63.4	0.05	103.43	1285.5	555.6	-2.8 deg/day	≈ 0 deg/day

Each orbit was propagated for four days in order to observe the changes in the right ascension of the ascending node and the argument of perigee. Since the rates shown in Table 1 agreed very closely with the predicted values it was felt that the J_2 equations were validated (2:157-158).

3.3 The Estimator

The estimator is a least squares differential corrector using a dynamics model based on two-body and J_2 effects. By using a Taylor Series approximation, the equations of state and the state transition matrix are expressed as explicit functions of time. Four different dynamics models are investigated by varying the order of the approximations used for the two-body and the J_2 parts of the equations. These variations are detailed in Table 2.

Table 2. Highest Order of Approximation in Equations of State

Estimator	Two-body Position / Velocity	J_2 Position / Velocity
ets4	4th / 3rd	None
ets4a	4th / 3rd	2nd / 1st
ets4b	4th / 3rd	2nd + 3rd / 1st + 2nd
ets5	5th / 4th	2nd + 3rd / 1st + 2nd

A different state transition matrix is derived from each set of state equations, except for 'ets5' which uses the same state transition matrix as 'ets4b'.

3.3.1 Program Execution. The input to the estimator program consists of the observation and ephemeris files generated by the truth program. Before the estimation process actually begins, all of the observations are read into an array for later use. During this process the program determines how many observations are in the file. By storing all of the observations in an array, the program does not need to read the observation file more than once thus reducing program run time. This approach also allows for the estimate to be epoched to the time of the middle observation which effectively doubles the time span over which the Taylor Series approximations to the equations of state are effective. After determining which observation is the *epoch observation*, the corresponding ephemeride can be read thus providing the true state at epoch.

A very simple technique is used to determine the initial reference state at the beginning of the estimation process. The position part of the reference state is immediately available from the epoch observation by converting the topocentric values to ECI coordinates (see Appendix A). The velocity part of the reference state is then found using two consecutive observations (epoch and epoch+1) by dividing the change in each position component by the time between observations:

$$\begin{aligned} u_{ref} &= \frac{x_{epoch+1} - x_{epoch}}{t_{epoch+1} - t_{epoch}} \\ v_{ref} &= \frac{y_{epoch+1} - y_{epoch}}{t_{epoch+1} - t_{epoch}} \\ w_{ref} &= \frac{z_{epoch+1} - z_{epoch}}{t_{epoch+1} - t_{epoch}} \end{aligned} \tag{44}$$

The estimator uses an iterative approach to correct the initial reference state into an estimate of the satellite's state at the epoch time. At the beginning of each iteration, the program calculates several "constants" based on the reference state for use in the equations of state and state transition matrix subroutines and initializes the running sum matrix and vector defined in Eq (31) and Eq (32).

As each observation is processed, a predicted observation is obtained by evaluating the equations of state using the difference between the observation time and the epoch time ($dt = t_{\text{observation}} - t_{\text{epoch}}$) and then converting from ECI to topocentric coordinates. The observation is then compared with the predicted observation and the residual calculated. The residuals for range, azimuth, and elevation are also used to update running sums for the mean and root mean squared (RMS) residuals:

$$\begin{aligned} sum &= \sum_{i=1}^N residual_i \\ sum2 &= \sum_{i=1}^N (residual_i)^2 \end{aligned} \tag{45}$$

The predicted state is next used to calculate the data linearization matrix **H** (see Appendix B) which is then combined with the state transition matrix to produce the observation linearization matrix $T = H\Phi$. After multiplying by the instrumental covariance matrix **Q** and the residual vector **r**, the results are added to the running matrix and vector sums found in Eqs (31) and (32).

When all of the observations have been processed, a new estimate of the state and its covariance matrix **P** is calculated using Eqs (29) and (33). Also the mean and RMS residuals are calculated for the *previous* estimate:

$$\begin{aligned} \text{mean residual} &= \frac{sum}{obcnt} \\ \text{RMS residual} &= \sqrt{\frac{sum2}{obcnt}} \end{aligned} \tag{46}$$

where *obcnt* is the total number of observations, *sum* is the cumulative residuals for all observations, and *sum2* is the cumulative residuals squared for all observations.

If the change in each element of the state is smaller than one-percent of its corresponding diagonal entry in the covariance matrix, then the estimator is considered to have converged. If not, then the estimate becomes a new reference state and the program loops back to start another iteration.

After convergence, the program calculates a new set of residual statistics by comparing each observation to predictions based on the new estimated state. The accuracy of the estimate is also calculated using the final estimated state and the true state to find the magnitude of the position and velocity errors at epoch:

$$\begin{aligned} r_{mag} &= \sqrt{(x_{truth} - x_{est})^2 + (y_{truth} - y_{est})^2 + (z_{truth} - z_{est})^2} \\ v_{mag} &= \sqrt{(u_{truth} - u_{est})^2 + (v_{truth} - v_{est})^2 + (w_{truth} - w_{est})^2} \end{aligned} \quad (47)$$

3.3.2 Development of the Taylor Series Approximations. As mentioned earlier, both the equations of state and the state transition matrix are approximated using a Taylor Series expansion in time. The primary advantage of taking this approach rather than numerically integrating the equations of motion and equations of variation is that the state and state transition matrix can easily be calculated at any given time. It was also felt that working with explicit functions of time would reduce the computational burden placed on the computer -- which is one of the caveats mentioned in Chapter 1.

To start with, the Taylor Series representation of the position and velocity of a satellite can be written:

$$\begin{aligned} \mathbf{r}(t) &= \mathbf{r}_0 + \mathbf{v}_0 dt + \frac{1}{2} \mathbf{a}_0 dt^2 + \frac{1}{6} \dot{\mathbf{a}}_0 dt^3 + \frac{1}{24} \ddot{\mathbf{a}}_0 dt^4 + \frac{1}{120} \dddot{\mathbf{a}}_0 dt^5 + O(dt^6) \\ \mathbf{v}(t) &= \mathbf{v}_0 + \mathbf{a}_0 dt + \frac{1}{2} \dot{\mathbf{a}}_0 dt^2 + \frac{1}{6} \ddot{\mathbf{a}}_0 dt^3 + \frac{1}{24} \dddot{\mathbf{a}}_0 dt^4 + O(dt^5) \end{aligned} \quad (48)$$

where $\mathbf{r}(t)$ is the satellite's position at some time t , $\mathbf{v}(t)$ is the satellite's velocity at some time t , \mathbf{r}_0 is the satellite's position at $t = 0$, \mathbf{v}_0 is the satellite's velocity at $t = 0$, and \mathbf{a}_0 is the satellite's acceleration at $t = 0$. The notation of using a subscript zero to indicate a condition at $t = 0$ will now be dropped and it will be understood that all quantities are evaluated at $t = 0$. As was done in section 3.2.2, the acceleration of the satellite can be broken into two parts, the two-body term and the J_2 term:

$$\mathbf{a} = \mathbf{a}_{2body} + \mathbf{a}_{J_2} \quad (49)$$

Rewriting Eq (34) as

$$\mathbf{a}_{2b} = -\frac{\mu \mathbf{r}}{r^3} \quad (50)$$

produces the second order term for the two-body dynamics. Differentiating with respect to time gives

$$\dot{\mathbf{a}}_{2b} = -\mu \begin{pmatrix} u/r^3 - 3x(ux + vy + wz)/r^5 \\ v/r^3 - 3y(ux + vy + wz)/r^5 \\ w/r^3 - 3z(ux + vy + wz)/r^5 \end{pmatrix} \quad (51)$$

which is the third order two-body term,

$$\ddot{\mathbf{a}} = -\mu \begin{pmatrix} a_x/r^3 - 3x(V^2 + rda)/r^5 - 6u(rdv)/r^5 + 15x(rdv)^2/r^7 \\ a_y/r^3 - 3y(V^2 + rda)/r^5 - 6v(rdv)/r^5 + 15y(rdv)^2/r^7 \\ a_z/r^3 - 3z(V^2 + rda)/r^5 - 6w(rdv)/r^5 + 15z(rdv)^2/r^7 \end{pmatrix} \quad (52)$$

which is the fourth order two-body term where

$$\begin{aligned} rdv &\equiv ux + vy + wz \\ rda &\equiv xa_x + ya_y + za_z \\ V &\equiv \sqrt{u^2 + v^2 + w^2} \end{aligned}$$

and finally

$$\ddot{\mathbf{a}} = -\mu \begin{pmatrix} -\mu u/r^6 + 45[u(rdv)^2 + x(rdv)(V^2 - \mu/r)]/r^7 - 9u(V^2 - \mu/r)/r^5 + 15\mu x(rdv)/r^8 - 105x(rdv)^3/r^9 \\ -\mu v/r^6 + 45[v(rdv)^2 + y(rdv)(V^2 - \mu/r)]/r^7 - 9v(V^2 - \mu/r)/r^5 + 15\mu y(rdv)/r^8 - 105y(rdv)^3/r^9 \\ -\mu w/r^6 + 45[w(rdv)^2 + z(rdv)(V^2 - \mu/r)]/r^7 - 9w(V^2 - \mu/r)/r^5 + 15\mu z(rdv)/r^8 - 105z(rdv)^3/r^9 \end{pmatrix} \quad (53)$$

which is the fifth order two-body term where

$$\begin{aligned}
a_x &= -\mu x / r^3 \\
a_y &= -\mu y / r^3 \\
a_z &= -\mu z / r^3
\end{aligned}
\tag{54}$$

Referring back to Eqs (39-42), the perturbative acceleration due to J_2 effects can be written as:

$$\mathbf{a}_{20} = -A \begin{pmatrix} 3x/r^5 - 15xz^2/r^7 \\ 3y/r^5 - 15yz^2/r^7 \\ 9z/r^5 - 15z^3/r^7 \end{pmatrix}
\tag{55}$$

which is the first order J_2 term for the Taylor Series.

Differentiating with respect to time gives:

$$\dot{\mathbf{a}}_{20} = -A \begin{pmatrix} 3u/r^5 - 15[2wxz + uz^2 + x(rdv)]/r^7 + 105xz^2(rdv)/r^9 \\ 3v/r^5 - 15[2wyx + vz^2 + y(rdv)]/r^7 + 105yz^2(rdv)/r^9 \\ 9w/r^5 - 45[wz^2 - z(rdv)]/r^7 + 105z^3(rdv)/r^9 \end{pmatrix}
\tag{56}$$

which is the second order Taylor Series term for the J_2 effect.

Development of the state transition matrix equations follows directly from the equations of state as:

$$\Phi(t, t_0) = \nabla_{\mathbf{x}(t_0)} \mathbf{h}(\mathbf{x}(t_0), t)
\tag{14}$$

where the function \mathbf{h} is given by Eq (48) as an explicit function of time. A complete derivation of the state transition matrix is given in Appendix C. It should be noted that the estimate is much more sensitive to the order of the equations of state than it is to the order of the state transition matrix (9:161).

3.3.3 Program Validation. The estimator program was validated by using it to estimate the state for orbital arcs taken from several test orbits. For these tests, the addition of noise and drag perturbations was "turned off" so that proper operation of the program could be verified. The orbital parameters for the six test orbits used are given in Table 3.

Table 3. Test Orbits for Estimator Validation

Orbit ID	Inclination (deg)	Eccentricity	Period (min)	Apogee Ht (km)	Perigee Ht (km)
A	35.26	0.3772	412.4	18895	5053
B	4.33	0.0010	89.45	254	241
C	93.06	0.0010	89.45	254	241
D	35.26	0.0819	98.06	1243	89
E	0.00	0.0000	88.93	222	222
F	7.33	0.0166	91.19	444	222

The major program modules that make up the program were also individually tested. This included the equations of state, the state transition matrix, the time conversion routines, the data linearization matrix **H**, and the routines to convert from topocentric to ECI and back.

The equations of state were tested by computing the state of a satellite at three second intervals using the Taylor Series equations and then comparing with the numerically integrated state using the equations of motion developed for the truth model. The state transition matrix was also tested by comparison to the numerically integrated matrix but only at two times ($dt = 3$ sec and $dt = 57$ sec). The matrix was first tested based only on two-body dynamics and once that was validated the J_2 terms were added. In order to test the J_2 terms, the value of the J_2 coefficient was temporarily changed to be the same as the earth's gravitational parameter so that the effects could more easily be seen. In order to get good agreement between the approximate and "exact" matrix it was necessary to use a third order expression for the J_2 perturbation. Of course, this degree of accuracy was not really needed since the true value of the J_2 coefficient is much smaller than the value for μ .

3.3.4 Determining the Order of the State Equations. Initially the two-body dynamics were modeled using a third order and a fourth order set of equations to see if there was much difference between them. The tests shown in Table 4 demonstrated that the fourth order equation was significantly better and so it was used as the basis for the equations of state and state transition matrix. For this test, the Taylor Series equations included only two-body effects while the truth data was generated using a numerical integrator with two-body, J_2 and drag effects. Errors were calculated by computing the vector magnitude of the difference between the two states.

Table 4. Position and Velocity Errors from 3rd and 4th Order Taylor Series

Test #	3rd Order T.S. Position Error (km)	3rd Order T.S. Velocity Error (cm/sec)	4th Order T.S. Position Error (km)	4th Order T.S. Velocity Error (cm/sec)
1	0.092	0.381	0.007	0.163
2	0.101	0.431	0.004	0.130
3	0.143	0.947	0.004	0.150
4	0.107	0.968	0.002	0.100
5	0.025	0.589	0.0001	0.017

- a. Tests 1 and 2 were run using test orbit E from Table 3.
- b. Tests 3-5 were run using test orbit F from Table 3.

After developing the first and second order equations for the J_2 perturbation, a different test was run to verify the equations and to provide some insight into their relative performance differences. For this test, a reference orbit was propagated using the Hamming numerical integrator and a time step of three seconds. This "true" value of the state was then compared to the predictions of three different equations of state and the results output as the magnitudes of the position and velocity errors (Rmag and Vmag). The three different equations of state were: (1) The fourth order two-body equations only ('eom4.for'). (2) The fourth order two-body equations plus the first order J_2 equations ('eom4a.for'). (3) The fourth order two-body equations plus the first and second order J_2 equations ('eom4b.for'). When the truth model included only the two-body dynamics 'eom4' performed the best. However, with the addition of J_2 and drag effects, it was quite obvious that the J_2 equations would be needed in the estimator. Figure 4 shows the relative performance of the three equations of state as a plot of their position error (Rmag) versus time (in timesteps).

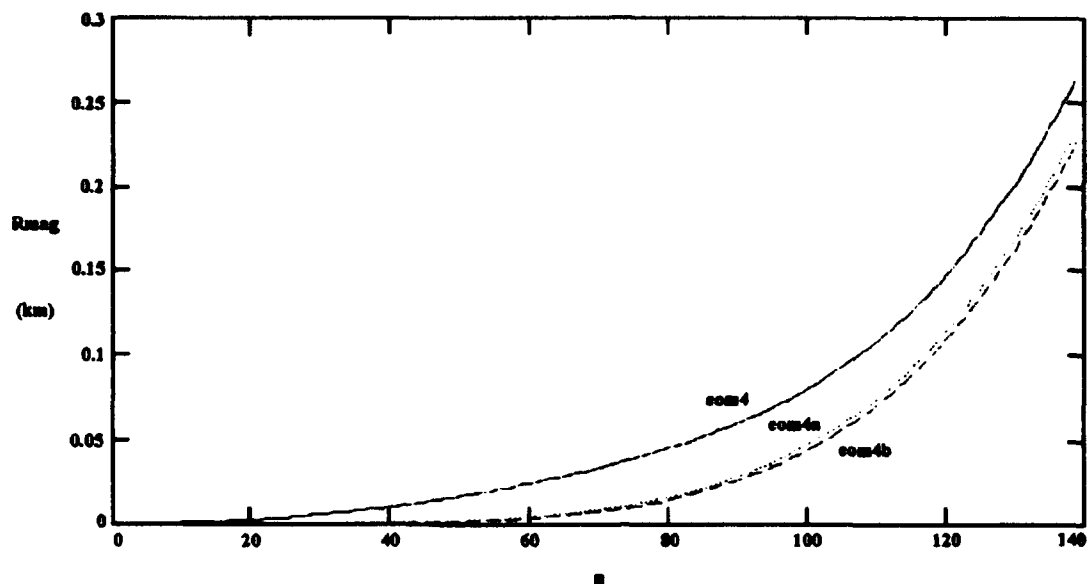


Figure 4. Position Error vs. Timestep for eom4, eom4a, and eom4b.

The data for Figure 4 was generated using test orbit A from Table 3. As can be seen, the plots show that a significant performance improvement occurs when J_2 is taken into account. There is very little difference between 'eom4a' and 'eom4b' but 'eom4b' is slightly better. This is expected since 'eom4b' uses a higher order approximation for J_2 effects.

However, for very low orbits, such as test orbits B through F in Table 3, 'eom4a' actually performs better than 'eom4b'. As can be seen in Figure 5 (generated from orbit C in Table 3), 'eom4b' is initially more accurate than 'eom4a', but after about 100 seconds 'eom4a' actually has a smaller error. This sort of behaviour is unexpected since it is normally expected that a higher order of approximation would give more accurate results.

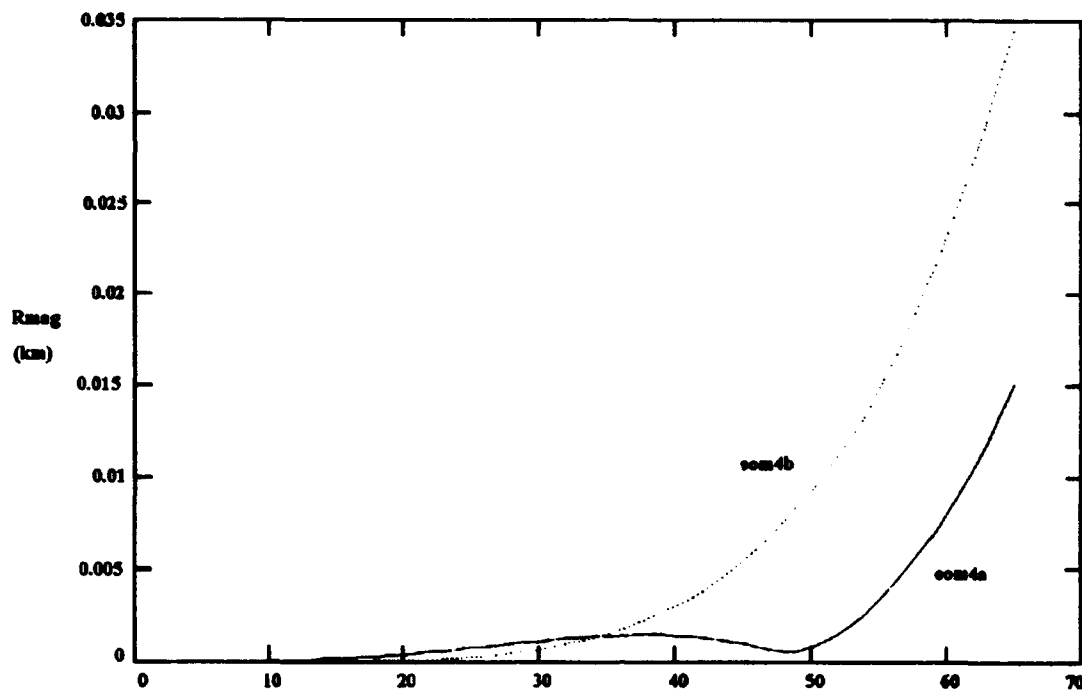


Figure 5. Position Error vs. Timestep for com4a and com4b.

Using a figure of merit that the position error should be within one kilometer, the duration during which each version of the state equation should be usable is given in Table 5.

Table 5. Effective Time Duration for State Equations

Orbit	com4	com4a	com4b
E	5:33	6:12	6:00
A	9:18	9:21	9:24
B	5:48	6:36	6:24

As can be seen, for very low orbits, 'com4a' is slightly better than 'com4b' and both of them are significantly better than 'com4'. However, at higher altitudes the difference between the three versions is very slight and the approximate equations of state are "good" for 50-70% longer.

3.4 Orbital Parameters.

All of the orbits mentioned so far were used only for development and testing of the programs used in this study. Analysis of the estimator performance was actually carried out using the orbits detailed in Tables 6 and 7.

Table 6. Orbital Elements - Satellite 20003

ECI State Vector			Classical Elements		
Epoch	Variable		Period	95	min
x pos	4961.174	km	Eccentricity	0.0001	
y pos	-4210.369	km	Inclination	28.5	deg
z pos	-2286.044	km	Rt. Ascension	0	deg
x vel	5.280	km/sec	Arg of Perigee	56	deg
y vel	4.806	km/sec	True Anomaly	260	deg
z vel	2.610	km/sec	Perigee Ht	517.9	km
			Apogee Ht	519.3	km

Table 7. Orbital Elements - Satellite 20004

ECI State Vector			Classical Elements		
Epoch	Variable		Period	110	min
x pos	1968.306	km	Eccentricity	0.0001	
y pos	-6455.632	km	Inclination	28.5	deg
z pos	-3505.122	km	Rt. Ascension	0	deg
x vel	6.993	km/sec	Arg of Perigee	25	deg
y vel	1.647	km/sec	True Anomaly	260	deg
z vel	0.894	km/sec	Perigee Ht	1225.9	km
			Apogee Ht	1227.4	km

The very low eccentricity is typical for low earth satellites that have been in orbit for any significant time and also eliminates the influence of apogee and perigee on the length of each pass. The inclination was chosen because it is typical of U.S. shuttle orbits and because it was high enough to ensure a ninety degree pass over the sensor site used in the study. The argument of perigee was chosen to put the perigee in the northern hemisphere which is where the sensor site is located. By setting the true anomaly to 260° the satellite is positioned for an ascending pass and will begin its trajectory outside the sensor's coverage. This reduces the length of the orbit which must be integrated before the satellite enters sensor coverage.

Satellite 20003 was used to evaluate the estimator performance on very low NE satellites. Track duration varied from about 6.5 minutes at very low elevation to 12.4 minutes at very high elevation. Satellite 20004 was chosen to evaluate estimator performance on relatively high NE satellites. Track duration varied from 10.2 minutes to 21.5 minutes. The inclination and eccentricity were kept constant so that the effects of altitude could be more clearly noted.

3.5 Parameters for Data Generation.

Three major parameters were used in structuring the data generation: (1) the duration of the pass, (2) the data rate in observations per second, and (3) the dynamics used in the estimator. The maximum elevation of a track is directly related to how long the satellite is visible to the site and therefore the amount of data available for the estimator. This relationship is not linear but follows the pattern shown in Figure 6.

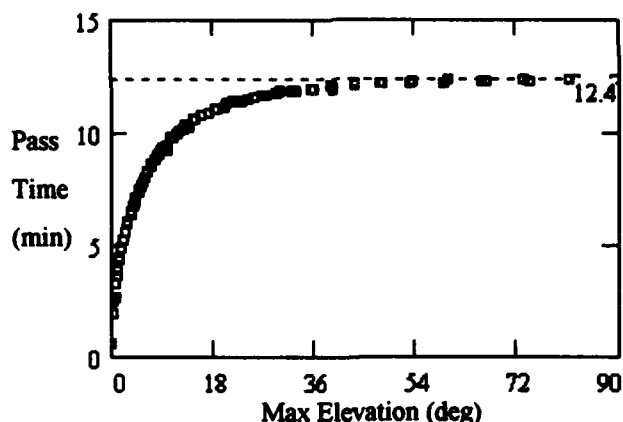


Figure 6. Plot of Pass Duration vs. Max Elevation

For a given sensor site, the exact relationship between the length of pass and maximum elevation is dependent on the satellite's orbit (shape and size) but will still have the basic shape exhibited in Figure 6. In order to characterize the relationship between estimator performance and pass length, data was collected using the schedule shown in Table 8. As shown in Figure 6, the duration of a pass changes more quickly at low elevation than at high elevation and after about 30 degrees there is relatively very little

change at all. Because of this, more passes were scheduled at the lower elevations than at the higher elevations.

Table 8. Schedule of Passes for Data Collection

Orbit	Param	A	B	C	D	E	F	G	H	I	J
20003	Time	6.60	7.56	8.37	9.65	10.41	11.36	12.08	12.28	12.45	n/a
"	EI	3.45	4.84	6.35	9.90	13.16	20.47	35.38	48.03	89.44	n/a
20004	Time	10.2	12.85	15.05	16.35	17.50	18.90	19.95	20.95	21.30	21.50
"	EI	3.60	6.28	9.77	12.64	16.03	22.36	30.80	47.24	65.22	87.72

- a. Time refers to the duration of the scheduled pass in minutes.
- b. EI refers to the max elevation of the scheduled pass in degrees.

The rate at which a space surveillance radar generates observations is influenced by several factors: the type of radar, the radar's operating frequency, and the range to the satellite. This makes it difficult to specify a single data rate as being representative of all the radars in the SSN. However, it can be assumed that a radar could easily be capable of generating at least two observations per second and perhaps as many as 100 observations per second (7:156). It should be noted that the maximum data rate that sensors are expected to transmit to the SSC is one observation every six seconds (10). Based on this information, data for this study was generated at two rates -- one observation every six seconds and two observations per second.

3.6 Experimental Procedure.

The first step was to determine the proper epoch from which to start the satellite's trajectory in order to obtain the desired maximum elevation during each pass. This was done using a program written expressly for this purpose. The output from this program gives: (1) an epoch for the state vector in Table 5, (2) the associated rise, culmination, and set times and elevation angles, and (3) the satellite's state and epoch one minute before entering sensor coverage.

Next, the resulting state vector and epoch was input into the truth model. By using the set time plus a safety margin the end time for the truth model propagation could be efficiently specified. The time step

was specified either in the input file or during program execution. The output from the truth model was then input into the four different estimators for processing.

The data generated by the estimators was then plotted to allow analysis and comparison of each estimator's performance.

3.7 Equipment.

The programs used in this study were written in Microsoft FORTRAN v5.1 and run on a 486DX PC running at 33 MHz. Some supplementary work and generation of graphs was done using Mathcad v3.1. Mathematica was used extensively in deriving the Taylor Series equations for the equations of state and the state transition matrix.

3.8 Summary.

The effectiveness of using a least squares batch estimator to estimate the state of a satellite is investigated using simulated observations from a single radar tracks. The observations are generated using a truth model that uses a fourth order numerical integrator to propagate the satellite's orbit for a small portion of the orbit. The estimator models the orbital dynamics using only two-body and J_2 effects using equations of state and state transition matrix that are expressed in explicit form using a Taylor Series approximation.

IV. Results and Analysis

4.1 Introduction

Four different versions of the estimator were compared using data from two different orbits, two different time steps, and two different noise settings (on and off). The results were examined to determine whether (1) the estimators were effectively compressing the data and (2) how accurate each estimator was. Analysis of the residuals was done after convergence to determine if the mean error was approximately zero and if the RMS error was close to the one sigma values for range, azimuth and elevation. Also of importance was the accuracy of the estimate as measured by the position and velocity errors relative to the true state.

While discussing the performance of the estimators it will be useful to refer to the first three estimators ('ets4', 'ets4a', and 'ets4b') as the *fourth order estimators*. This is because their behavior tends to be quite similar and all three are based on the fourth order Taylor Series approximation of the two-body equations of motion. Likewise the last estimator, 'ets5', will sometimes be referred to as the *fifth order estimator*.

Because of the non-linear relationship between track length and maximum pass elevation, it is necessary to look at the results from both perspectives. As an example, track lengths for the low orbit used in this study range from 6.5-12.4 minutes. An estimator may give good results for tracks up to 11.3 minutes long -- which would seem to cover a significant portion of the possible passes. However, in terms of pass elevation this would translate to good performance only for passes with a maximum elevation of 20 degrees or less.

4.2 Estimator Performance Using Perfect Data.

Data rate proved to be unimportant when the estimators were provided with noiseless data. The RMS and mean residual statistics along with the position and velocity errors were practically identical

regardless of data rate and varied by only a few percent. Because of this, only information from the low data rate will be presented and discussed for both the low and high orbits.

4.2.1 Low Orbit. Figures 7 and 8 show the RMS and mean error statistics of each estimator versus track length for the low orbit (satellite 20003). Figures 9 and 10 present this same information plotted against the maximum elevation of the pass. As can be seen from these figures, 'ets5' consistently outperforms the other three estimators with RMS and mean residuals that are approximately zero for all passes. Although the azimuth and elevation residuals for the fourth order estimators diverge significantly away from zero, they are still relatively small. However, the range residuals indicate a definite weakness in that parameter. All three of the fourth order estimators either exceed or approach RMS residuals of 100 meters for passes that last 12.2 minutes or more -- which equates to elevations of 48 degrees or greater.

The RMS and Mean residuals indicate that the *interval of convergence* of the fourth order estimators is significantly less than most of the track durations looked at in the low orbit. Residuals for observations that occur in a small time interval (the interval of convergence) centered around the estimate's epoch time are rather small while residuals for observations outside this interval increase rapidly as Δt increases. As the track length increasingly exceeds the interval of convergence, the percentage of the total residuals outside the interval also increases as does their magnitude. Eventually these large residuals become significant and cause the RMS and Mean residuals to diverge away from zero. The fifth order estimator performs well because its interval of convergence is significantly larger. However, it should be noted that even the fifth order estimator's residuals show a slight divergence away from zero. Even though the interval of convergence is larger it is still finite.

Figures 11 and 12 show the position and velocity errors in the estimated state from each estimator versus track length and maximum pass elevation respectively. Again, the fifth order estimator significantly outperforms the other estimators. Interestingly, while the velocity error increases with track length for 'ets4a' and 'ets4b', it *decreases* for 'ets4'. For tracks longer than 11 minutes (about 18 degrees in elevation) 'ets4' actually produces *smaller* velocity errors than both 'ets4a' and 'ets4b'. The maximum

error produced by 'ets5' is 1.8 meters in position and 2.2 cm/sec in velocity. A more quantitative analysis of the information contained in the graphs is presented in Table 9. Because of the very different shape of the curves depending on whether the errors are plotted against time or elevation, weighted averages were calculated for each case. Table 9 shows that the average velocity error for 'ets4' is still worse than any of the other estimators.

Table 9. Position and Velocity Errors from Perfect Data -- Low Orbit

Estimator	Position Error (m)				Velocity Error (cm/sec)			
	Min	Max	Avg vs Time	Avg vs Elevation	Min	Max	Avg vs Time	Avg vs Elevation
ets4	46.1	128.9	77.8	80.4	44.5	104	63.5	53.1
ets4a	0.7	60.2	18.2	26.6	6.7	64.3	26.4	33.3
ets4b	1.4	79.9	24.5	35.7	9.8	89.7	37.1	47.2
ets5	0.3	1.8	0.9	0.9	0.3	2.3	1.1	1

Normally, it is expected that as the track duration increases the accuracy of the estimated state will also increase since more data is available for the estimator. However, as can be seen in Figure 11, this is not true for the fourth order estimators. As was the case for the residuals, the interval of convergence for these estimators is too small and so estimates of the state become worse as the track duration increases.

The unexpected trend in velocity errors for 'ets4' relative to 'ets4a' and 'ets4b' could possibly be related to changes in the value for the J_2 potential function. Recollect that the J_2 potential function is given by Eq (40). If the potential at the middle of the track is considered indicative of the potential over the entire span of the track, then a comparison of the potentials associated with each pass will show that at 12 minutes (Pass #7) the J_2 potential function is a minimum. This could possibly reduce the importance of the J_2 terms contained in 'ets4a' and 'ets4b'. Additionally, the J_2 terms could have the effect of adding *numerical noise* to the state predictions. This could be a factor in explaining why 'ets4' gives better velocity estimates than the other fourth order estimators for passes longer than 10.5 minutes.

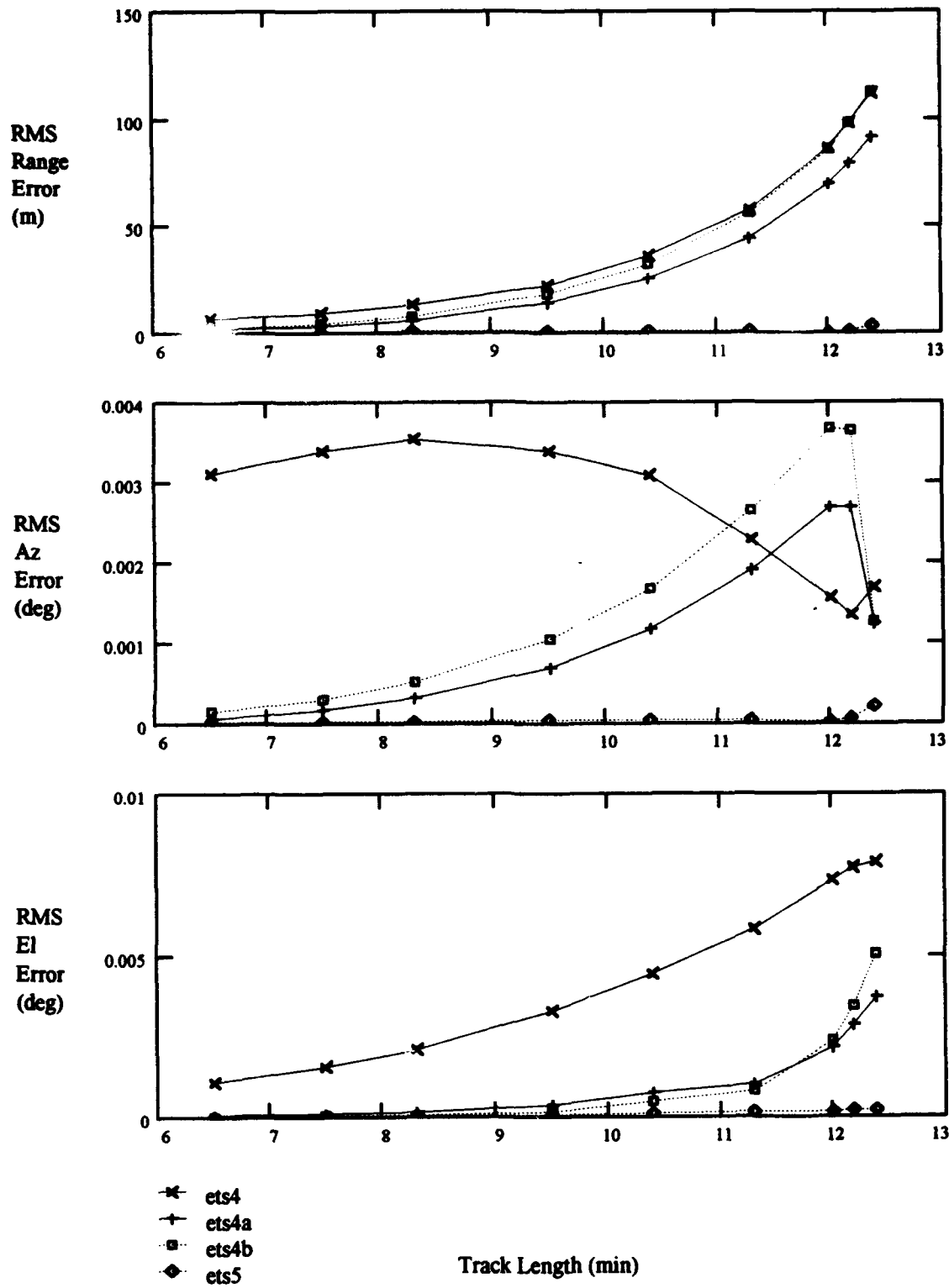


Figure 7. Converged RMS Residuals vs. Track Length – Low Orbit

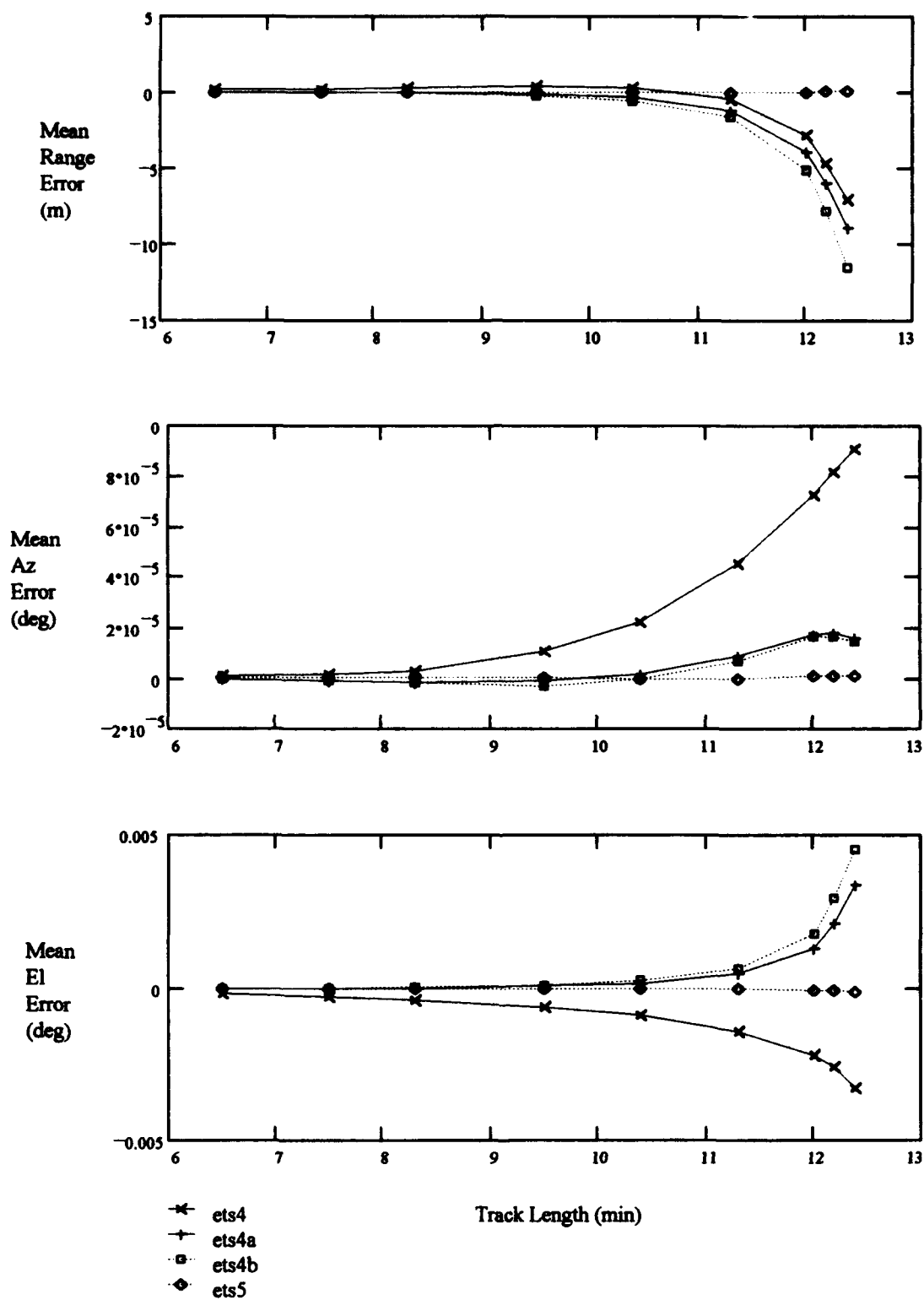


Figure 8. Converged Mean Residuals vs. Track Length -- Low Orbit

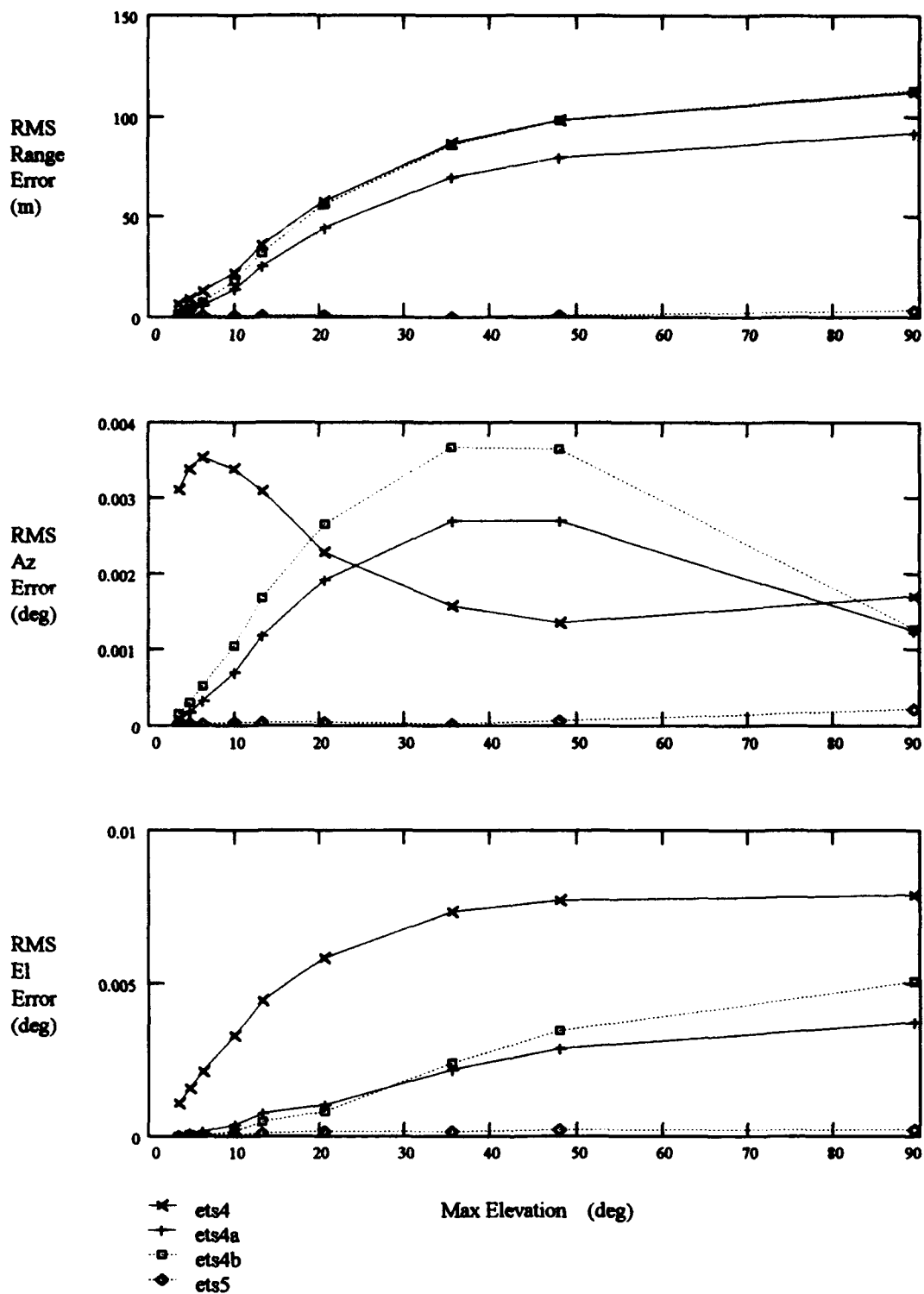


Figure 9. Converged RMS Residuals vs. Max Elevation -- Low Orbit

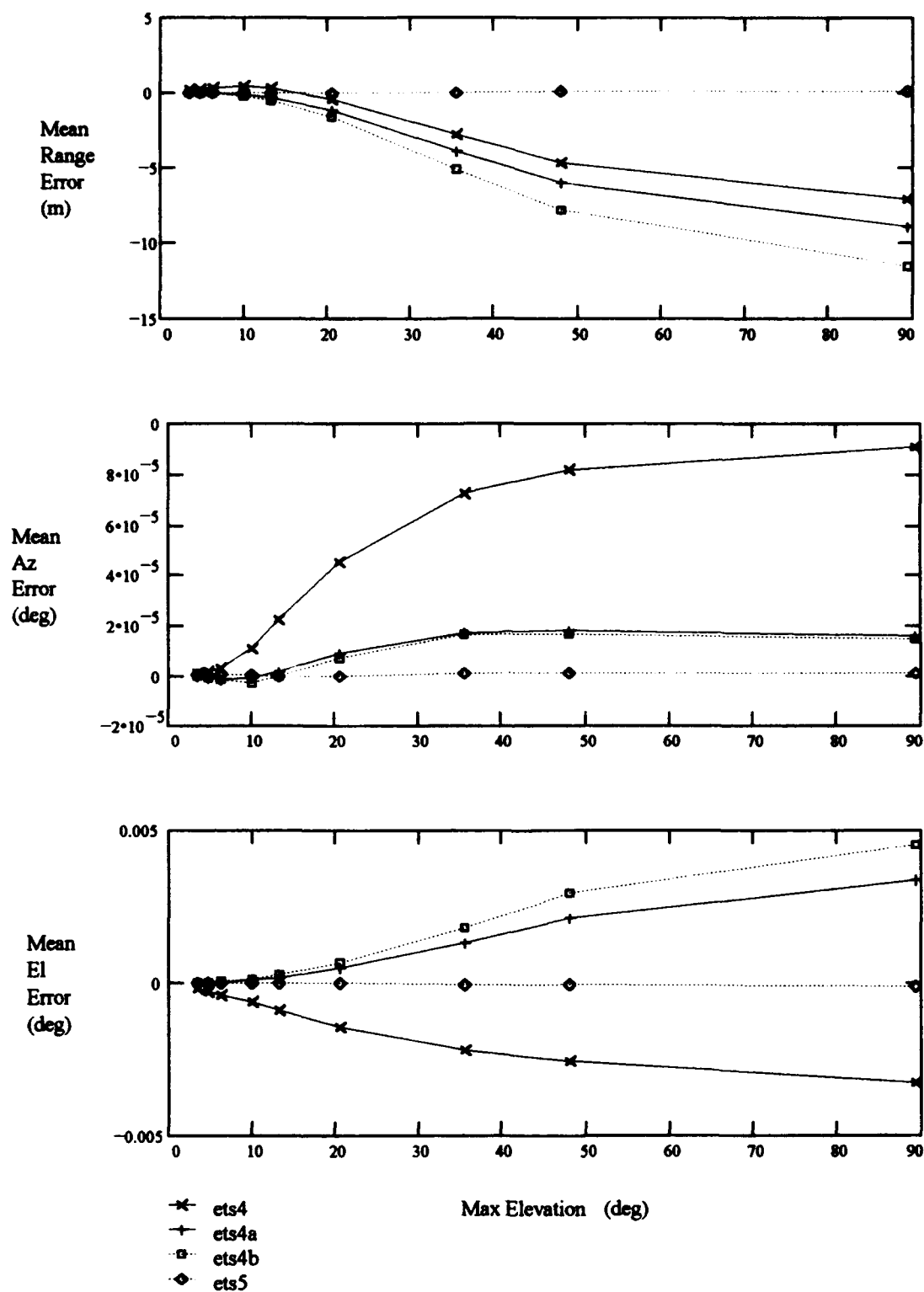


Figure 10. Converged Mean Residuals vs. Max Elevation -- Low Orbit

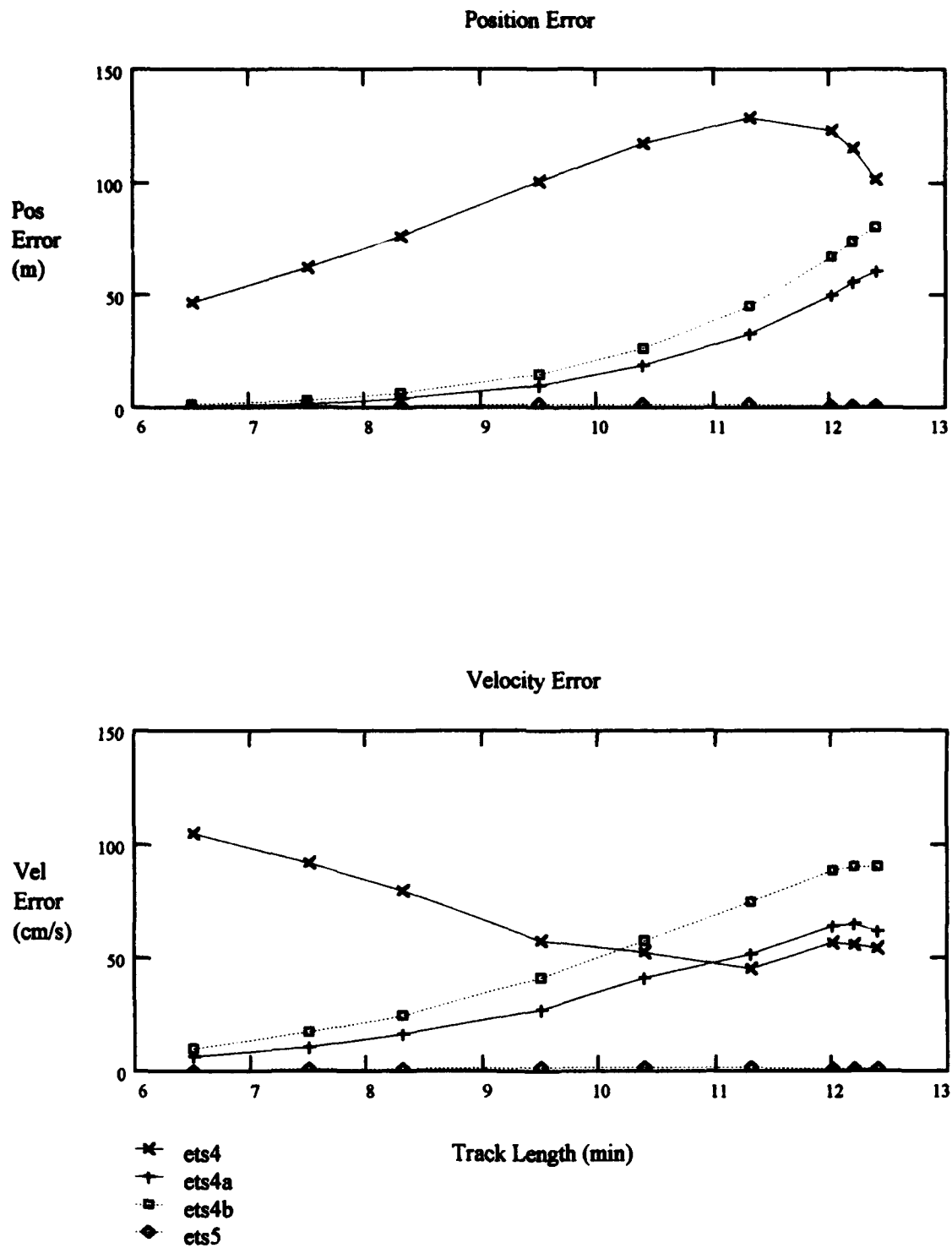


Figure 11. Position and Velocity Errors vs. Track Length -- Low Orbit

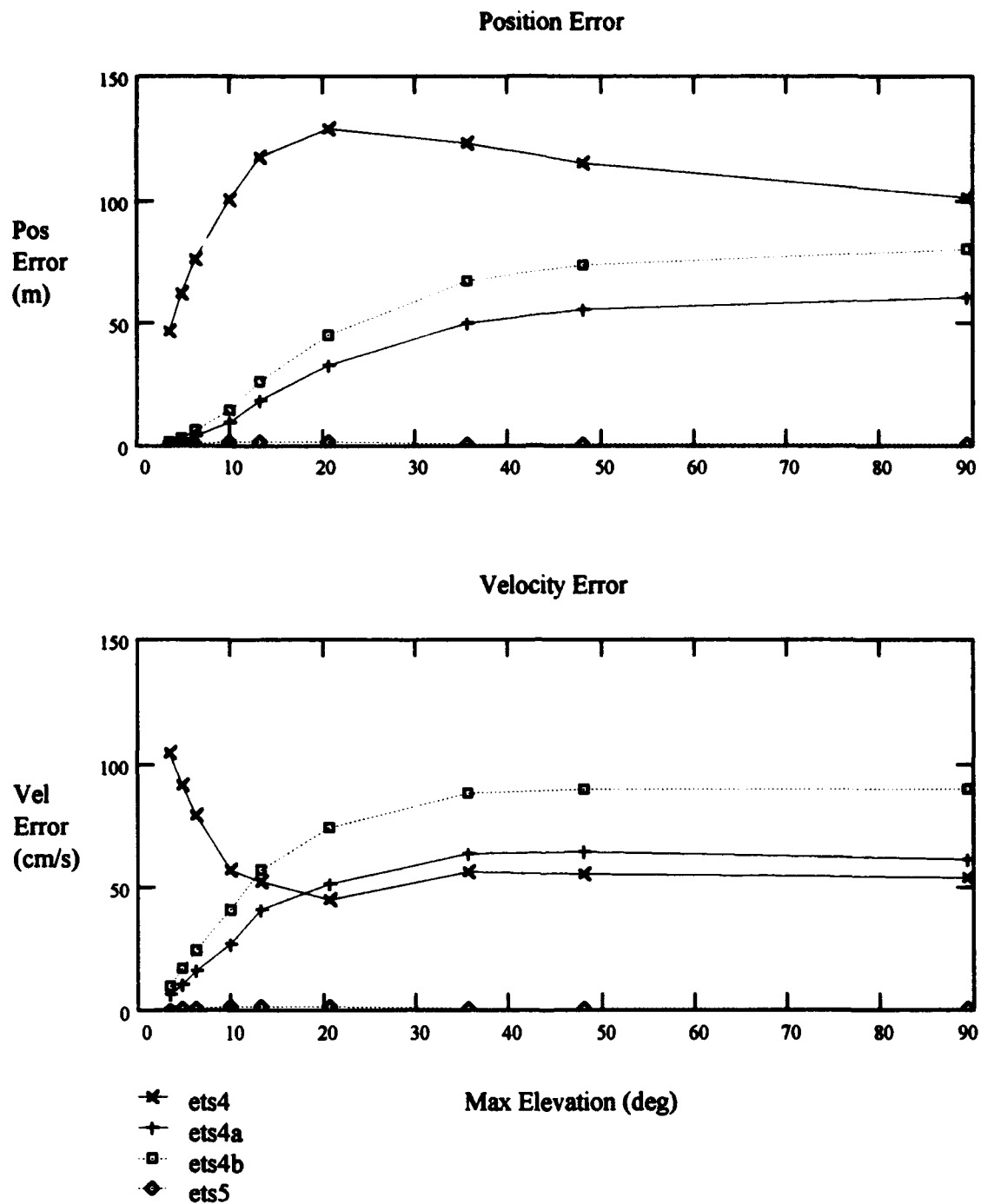


Figure 12. Position and Velocity Errors vs. Max Elevation -- Low Orbit

4.2.2 High Orbit. Figures 13 and 14 show the RMS and mean error statistics of each estimator versus track length for the high orbit (satellite 20004). Figures 15 and 16 present this same information plotted against the maximum elevation of the pass. As can be seen from these figures, 'ets5' continues to significantly outperform the other three estimators.

The fourth order estimators show a definite inability to handle the significantly longer track durations. Elevation residuals, both RMS and mean, approach the one sigma value of 0.025 degrees at elevations above 60 degrees (pass length of 21 minutes) and exceed 0.01 degrees for passes above 30 degrees (20 minutes). Azimuth residuals are also very high, but exhibit some interesting behavior. The RMS residuals for azimuth have a maximum for tracks lasting about 21 minutes (max elevation of 48 degrees) and approach the 'ets5' value at pass elevations close to 90 degrees. For passes between 15-80 degrees, 'ets4' actually has a lower RMS value for azimuth residuals than either 'ets4a' or 'ets4b'. The mean residual values peak for tracks lasting about 17.5 minutes (16 degrees elevation) and pass through zero for 20 minute (30 degree) passes before once again increasing. Range residuals, both RMS and mean, show a steady growth with respect to time and elevation. The maximum RMS residuals go as high as 900 meters and the one sigma value of 100 meters is exceeded for tracks lasting longer than 17.5 minutes (about 16 degrees elevation).

Figures 17 and 18 show the position and velocity errors in the estimated state from each estimator versus track length and maximum pass elevation respectively. As expected, the fifth order estimator significantly outperforms the other estimators. Again, 'ets4' had smaller velocity errors than 'ets4a' or 'ets4b' after the track length had increased to a certain level. In this case, the crossover point was at a track length of about 14 minutes (8 degrees in elevation). As was seen for the range residuals earlier, the fourth order estimators show rapid growth in position and velocity errors to very high levels. Position errors exceeded 100 meters for tracks of 14 minutes (about 10 degrees elevation) or more. The information in Table 10 provides a quantitative look at this data for comparative purposes. Because of the very different shape of the curves depending on whether the errors are plotted against time or elevation, weighted averages were calculated for each case.

Table 10. Position and Velocity Errors from Perfect Data -- High Orbit

Estimator	Position Error (m)				Velocity Error (cm/sec)			
	Min	Max	Avg vs Time	Avg vs Elevation	Min	Max	Avg vs Time	Avg vs Elevation
ets4	29.3	755.4	251.7	348.2	89.1	380.7	174.8	215.9
ets4a	6.7	657.2	186.4	285.1	26.9	396.4	142.3	190.7
ets4b	7.2	722.9	205.3	314.2	29.4	449.3	160.6	215.9
ets5	2	23.6	9.3	9.5	1.5	21.7	8.9	8

The same relationship between track length and order of approximation in the equations of state that was seen for the low orbit is even more evident in the high orbit -- both for residuals and for accuracy. It should also be noted that 'ets5' and 'ets4b' both use the same state transition matrix but 'ets5' uses a higher order approximation for the equations of state. Therefore, the dramatic improvement in performance between the two estimators demonstrates that estimator performance is more sensitive to the "accuracy" of the equations of state than to the state transition matrix.

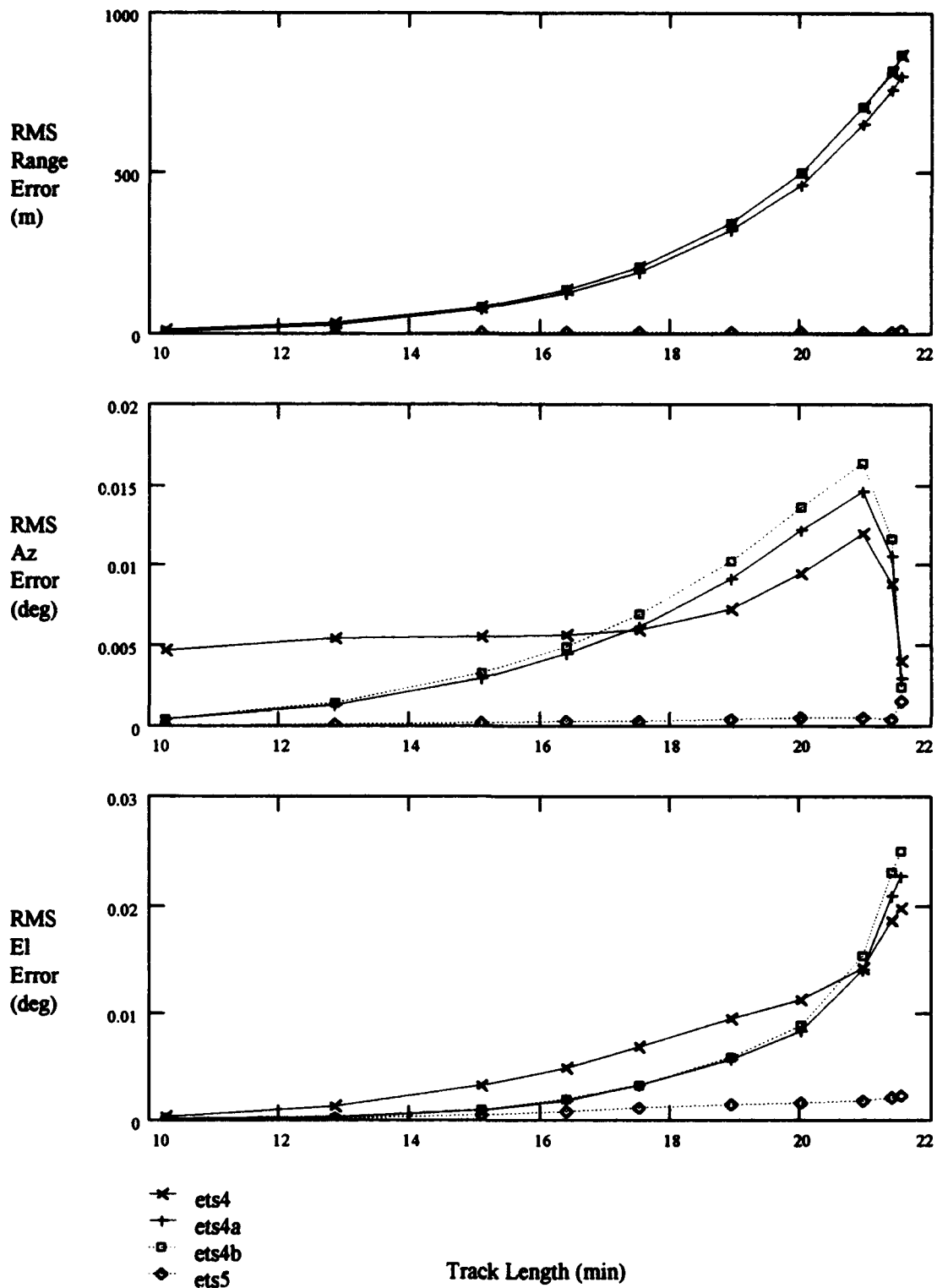


Figure 13. Converged RMS Residuals vs. Track Length -- High Orbit

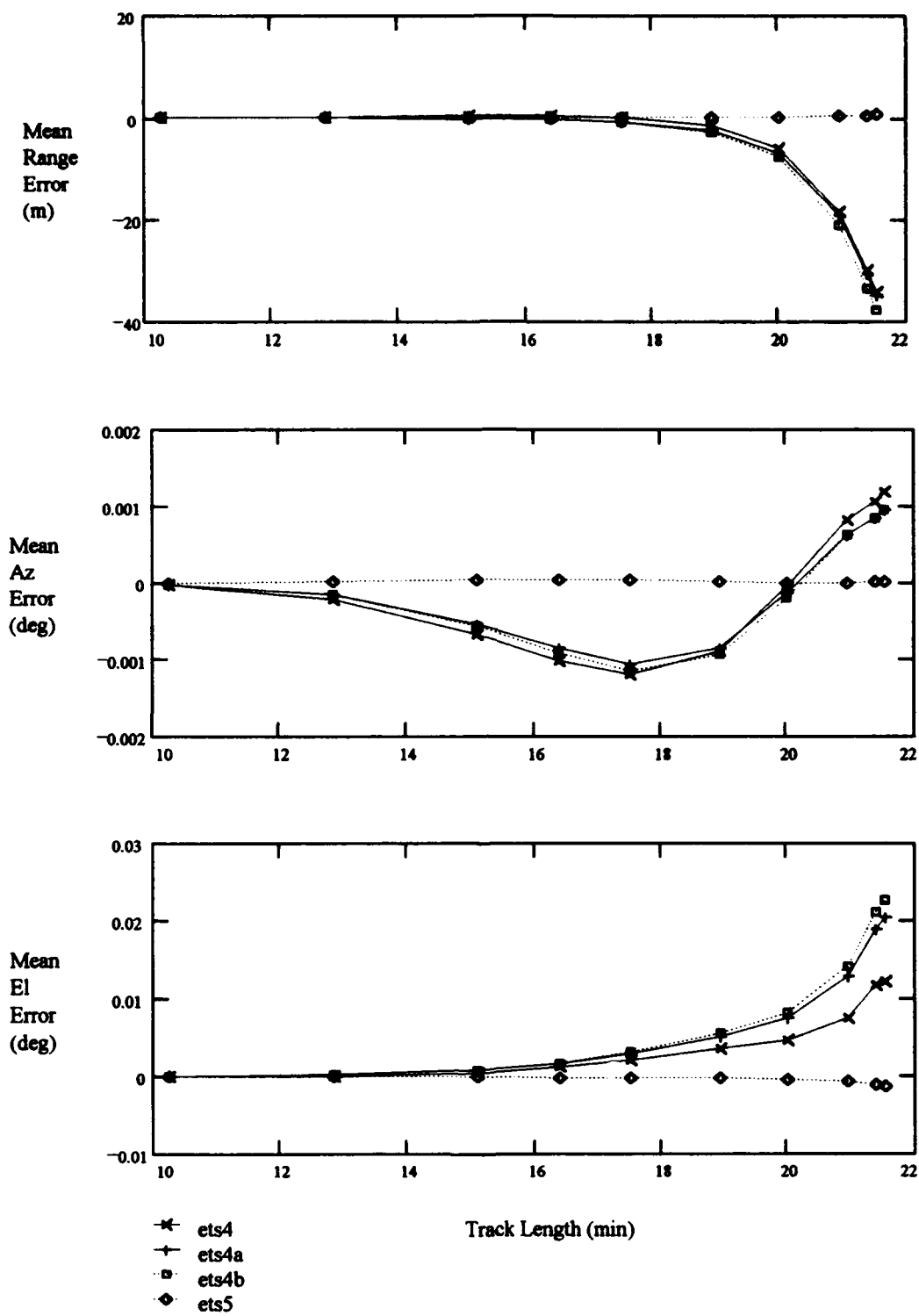


Figure 14. Converged Mean Residuals vs. Track Length – High Orbit

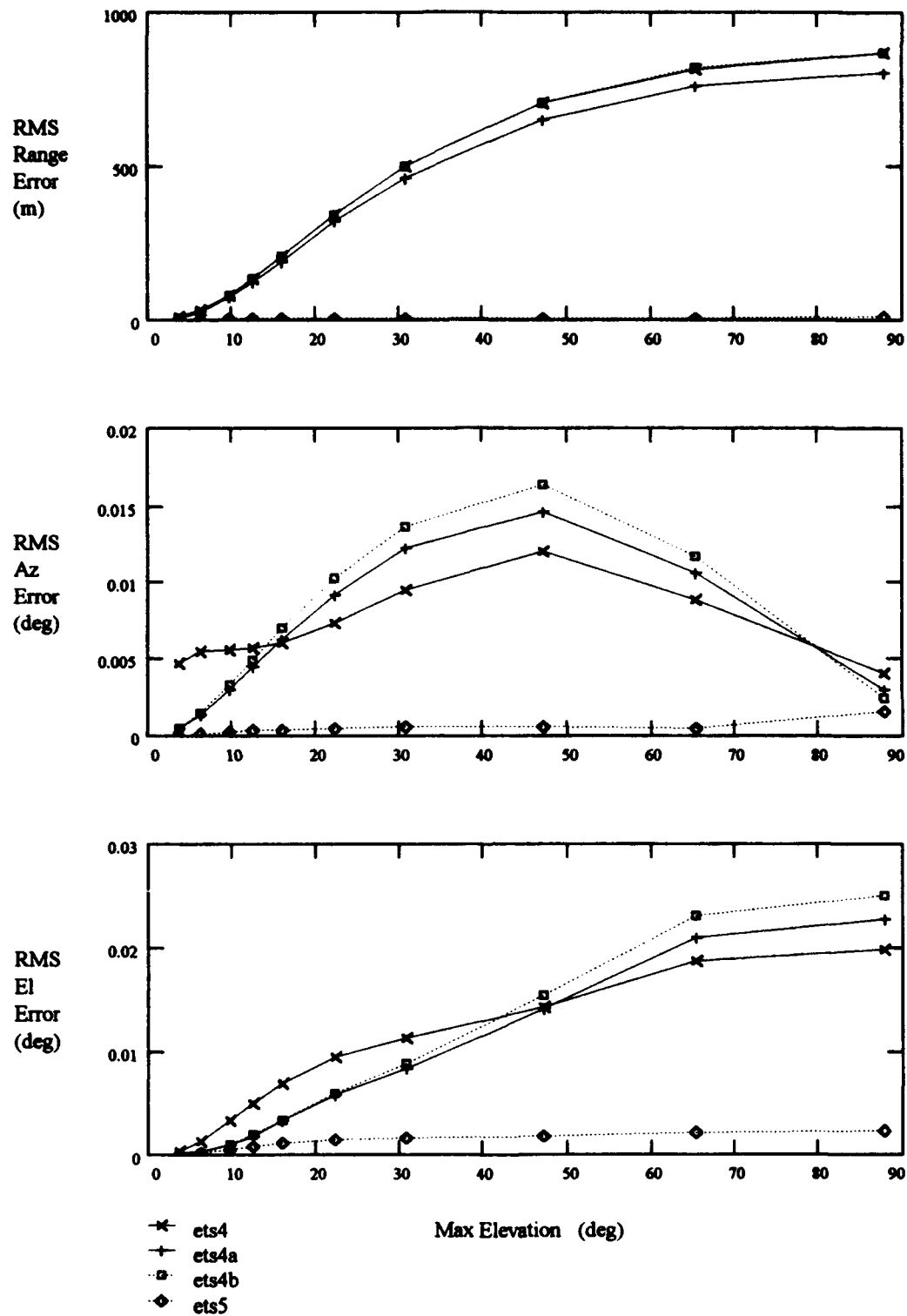


Figure 15. Converged RMS Residuals vs. Max Elevation -- High Orbit

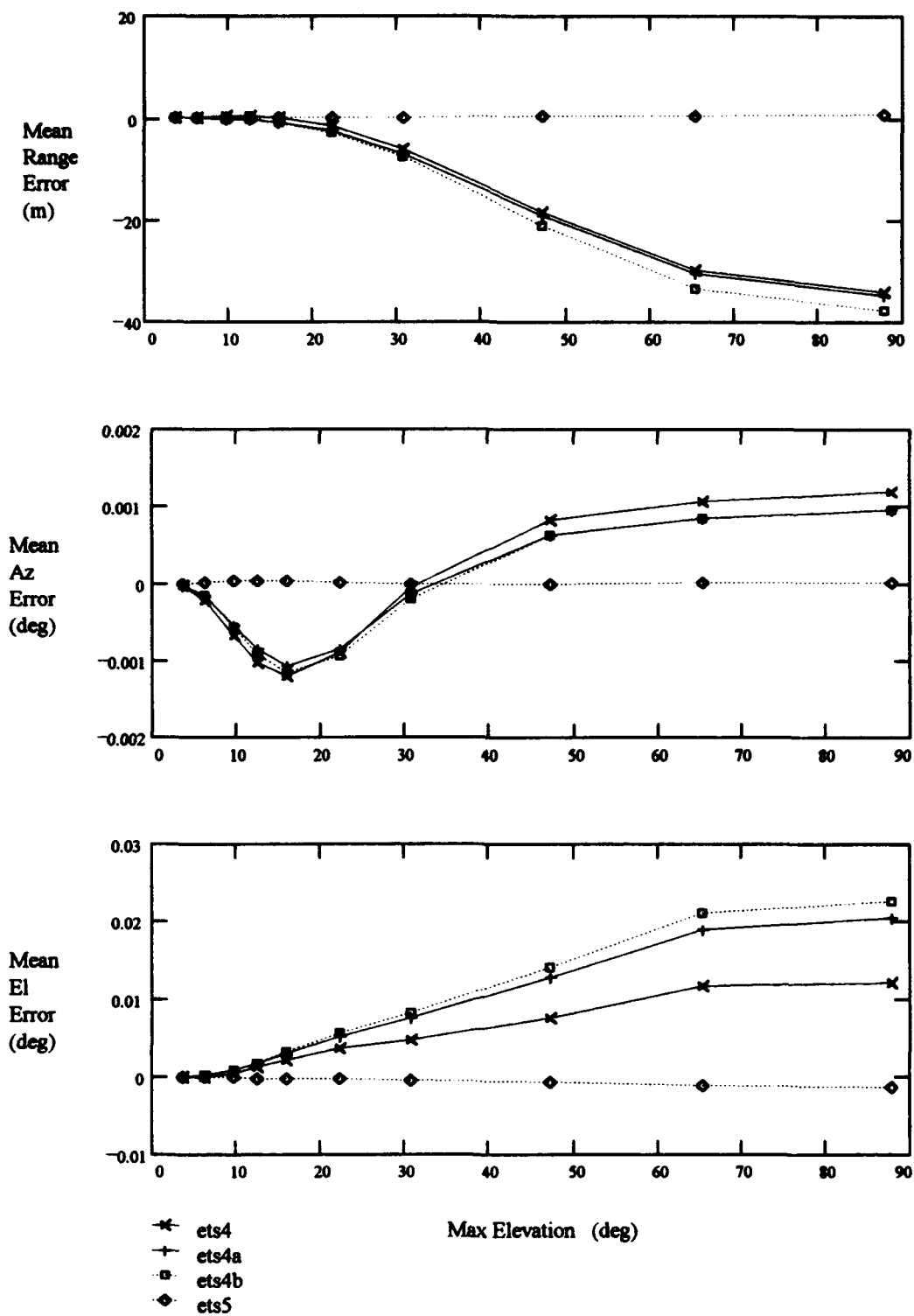


Figure 16. Converged Mean Residuals vs. Max Elevation -- High Orbit

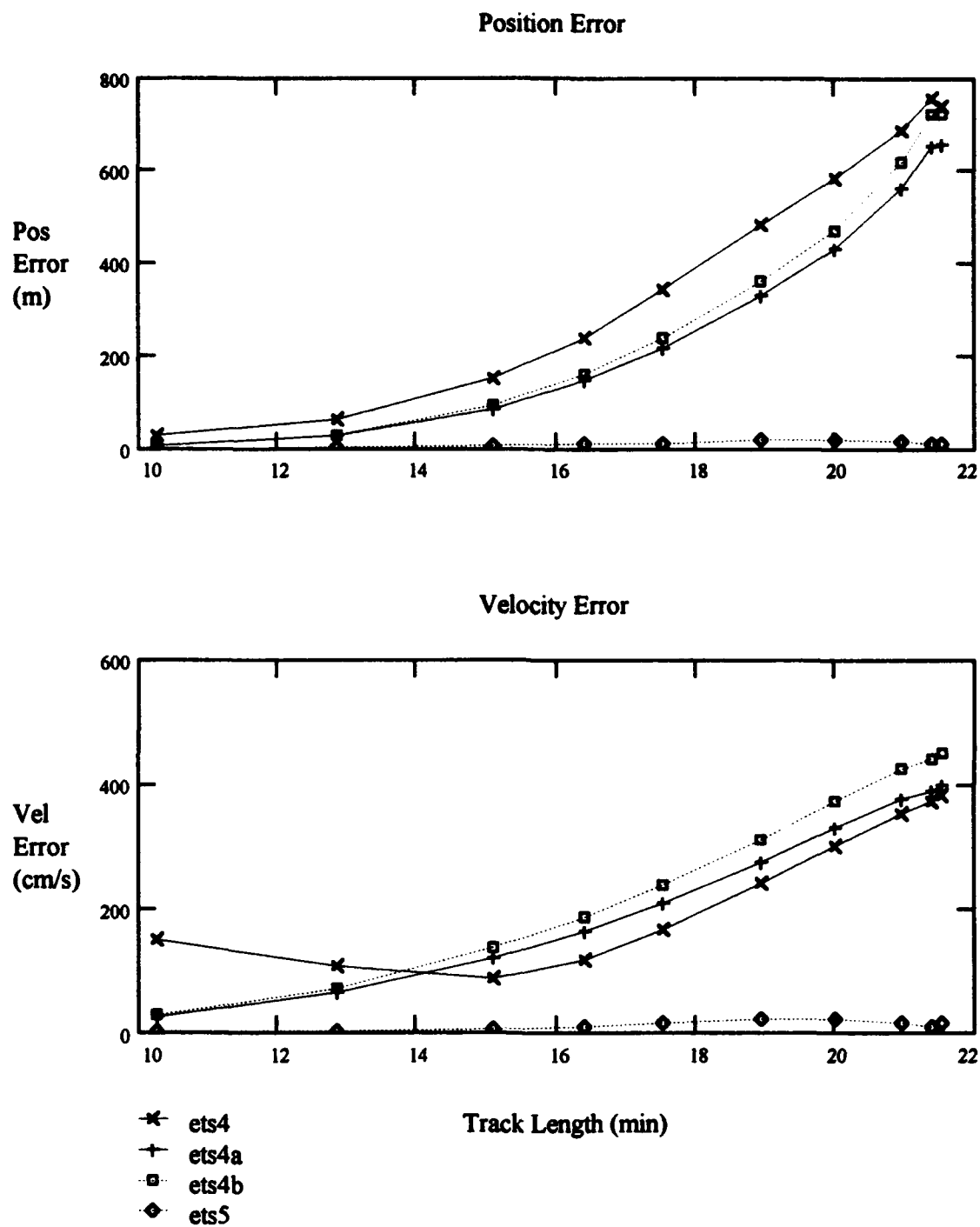


Figure 17. Position and Velocity Errors vs. Track Length -- High Orbit

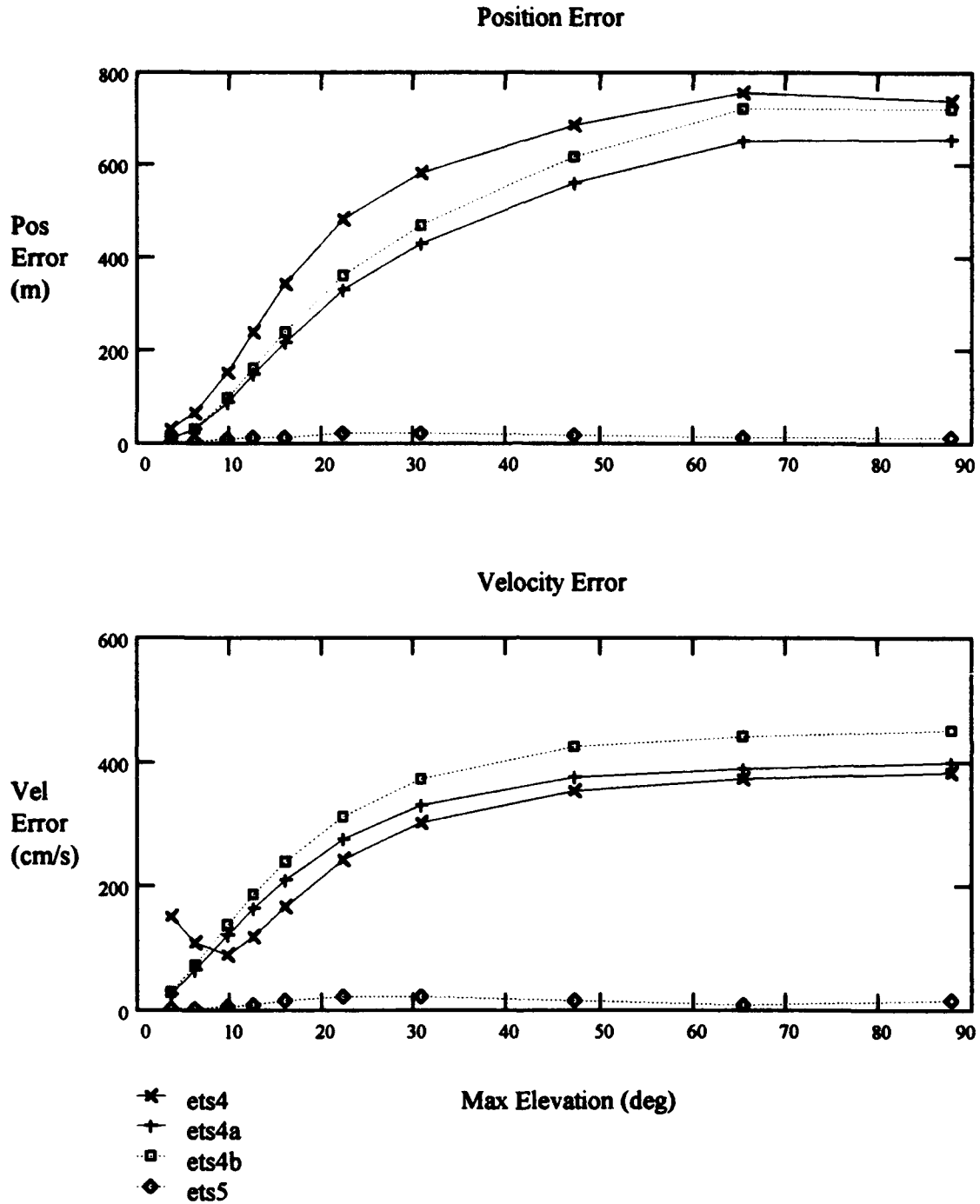


Figure 18. Position and Velocity Errors vs. Max Elevation -- High Orbit

4.3 Estimator Performance Using Noisy Data

In order to ensure that the random number generator had not biased the data to give especially good or poor results, several *data runs* were performed for each combination of orbit and data rate and the results averaged together. Each data run used a different initial *seed number* for the random number generator so that a totally different set of random numbers were generated during each data run. Twelve data runs were done for both the high and low orbits using the fast data rate. Five runs were done for each orbit using the slow data rate.

Testing of the estimators using noise-less data indicated that only the fifth order estimator was suitable for use. Because of this the fourth order estimators were dropped from further analysis and only the fifth order estimator was analyzed using noisy data.

It was observed that when the observations contained no noise, the data rate was not a factor in estimator performance. However, when the observations do include noise, the higher data rate results in better estimator performance.

4.3.1 Residuals. A typical plot of the average mean and RMS residuals for range, azimuth and elevation versus maximum pass elevation after convergence is shown in Figure 19. As can be seen, the average mean residuals are all very close to zero and the RMS residuals are all very close to their expected one sigma values. This behavior, with only minor differences, was exhibited in all cases regardless of orbital height, data rate, maximum pass elevation or track duration.

Figure 20 shows a typical plot of the RMS residuals before and after differential correction. Although, the final pass RMS residuals all seem to be zero, they are actually the same as in Figure 19. The size of the pre-correction RMS residuals dominates the vertical scale thus causing the post-correction values to appear to be zero.

Figures 21 and 22 shows the actual pre and post correction residuals in range, azimuth, and elevation for single passes of satellite 20004 over the site. Figure 21 is a minimum elevation pass (elevation = 3.6 deg) while Figure 22 is a maximum elevation pass (elevation = 87.7 deg). Both passes were generated using the fast data rate. Again, these plots are typical of all the cases looked at. The

"spike" in the first pass residuals seen in Figure 22 are caused by the rapid change in azimuth and elevation as the satellite passes almost directly overhead of the site. As can be seen, in comparison to the pre-correction residuals, the residuals after correction are very small and are approximately zero.

Figure 23 plots the low elevation pass post-correction residuals used in Figure 21 versus their expected one sigma limits. Although outliers exist, the greater majority of residuals lie within the one sigma limits. It should also be noted that the outliers all appear to be within three sigma of zero. This is exactly what is expected since after correction the major source for the residuals should be the noise that was in the observations.

All of the information presented in Figures 19-23 indicates that the fifth order estimator has effectively extracted all of the pertinent information from the observation data.

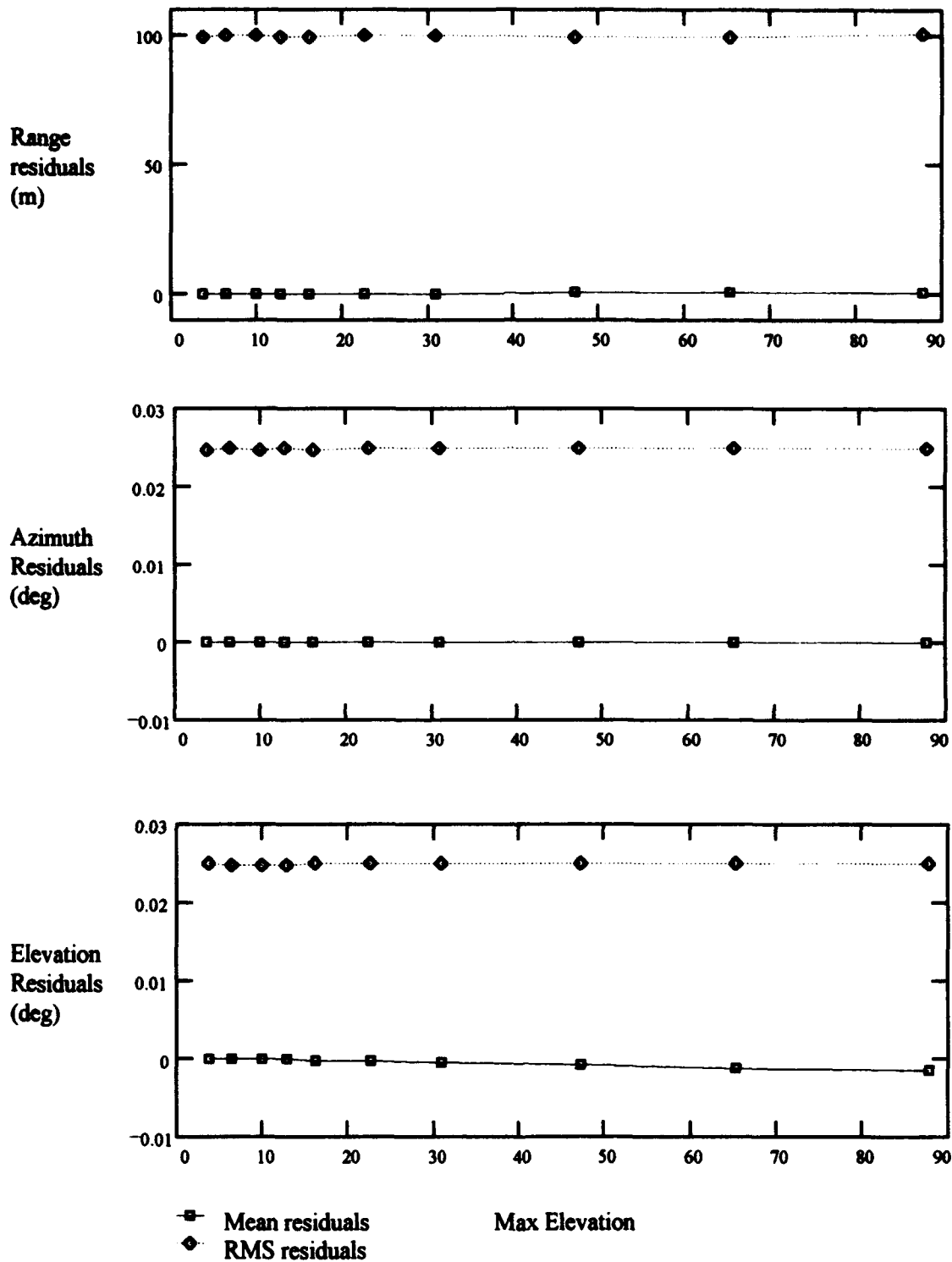


Figure 19. Average Mean and RMS Residuals After Convergence versus Max Elevation

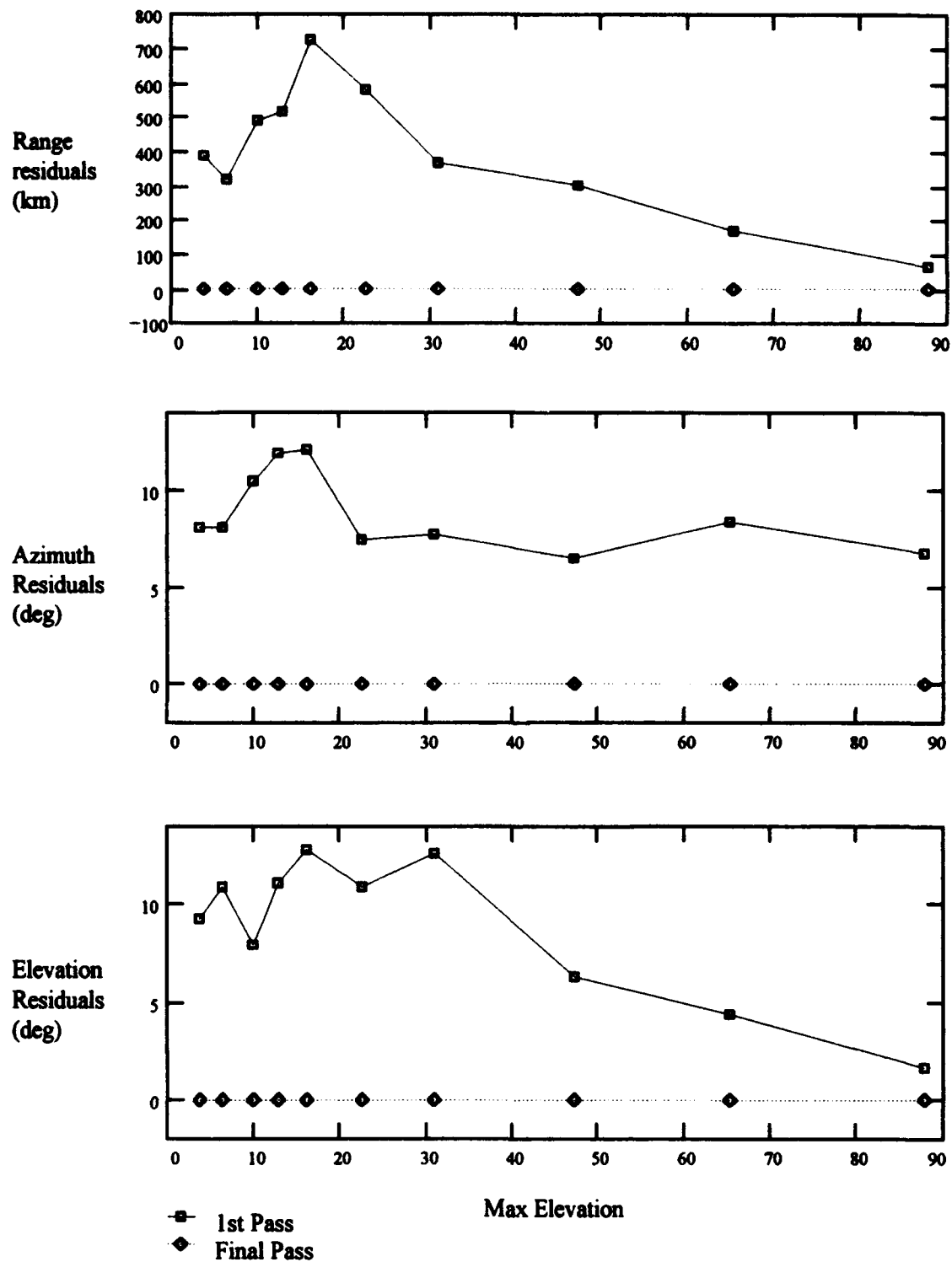


Figure 20. Average RMS Residuals Before and After Correction versus Max Elevation

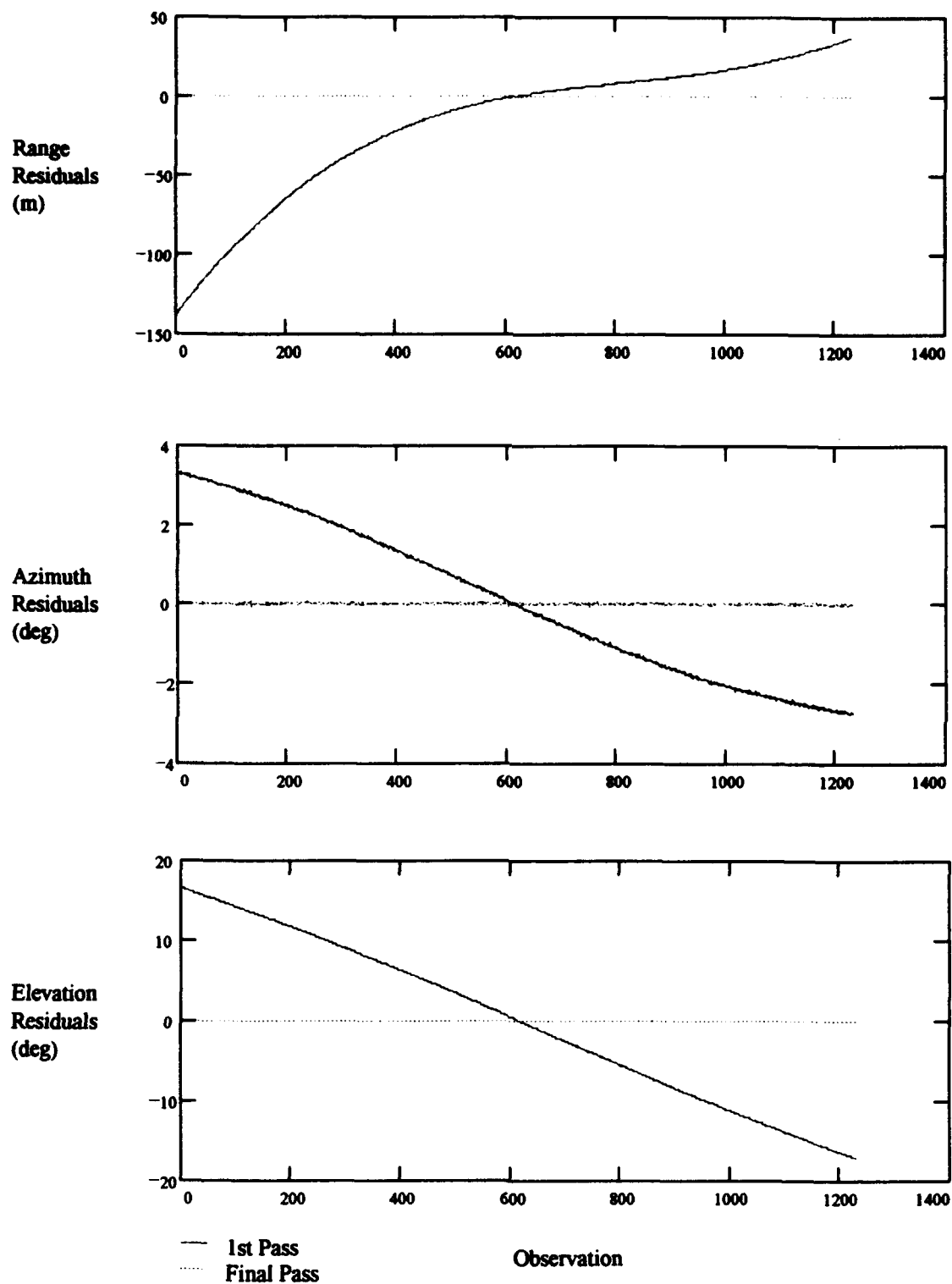


Figure 21. Residual Values Before and After Correction - Low El Pass

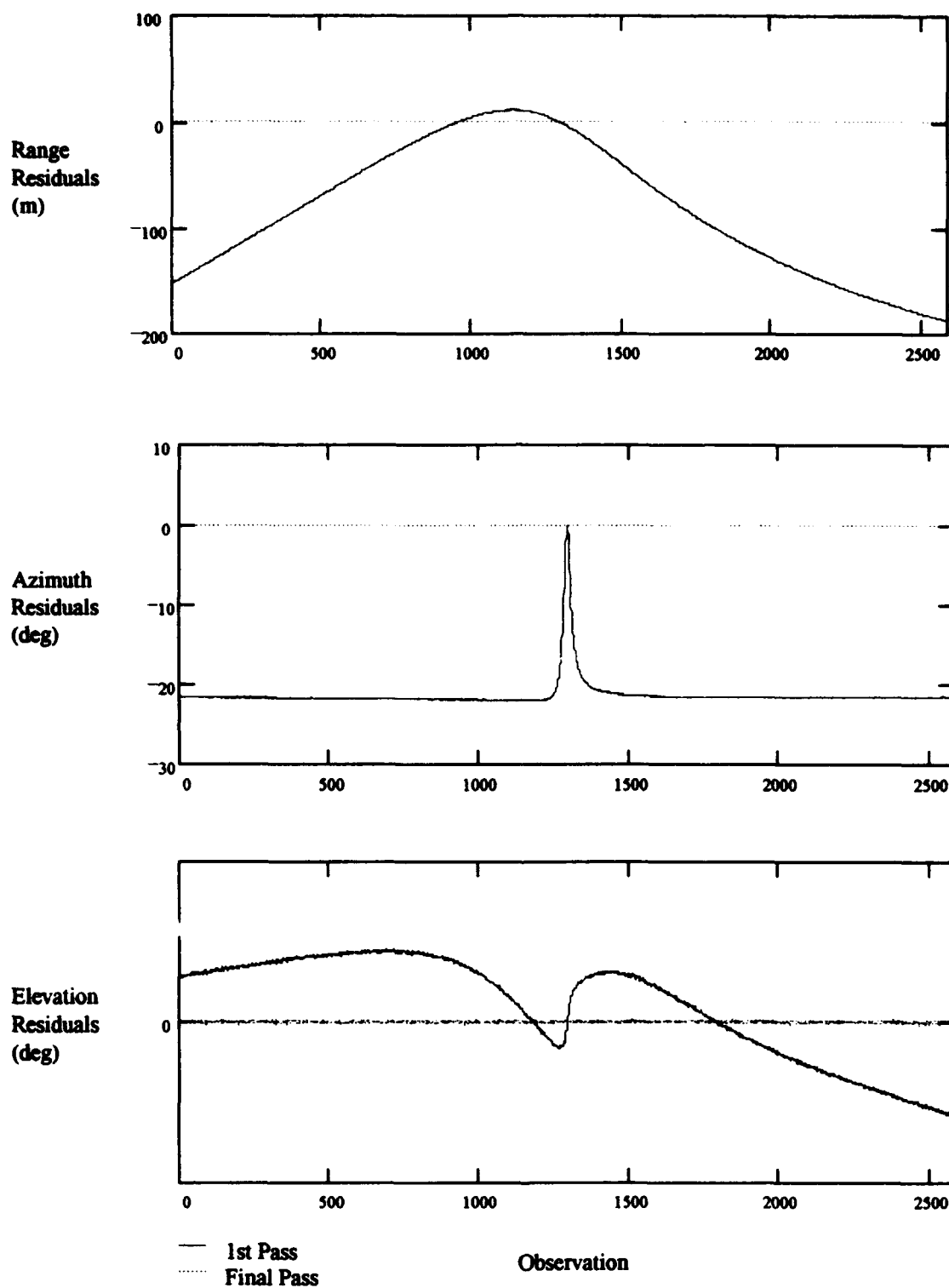


Figure 22. Residual Values Before and After Correction - High El Pass

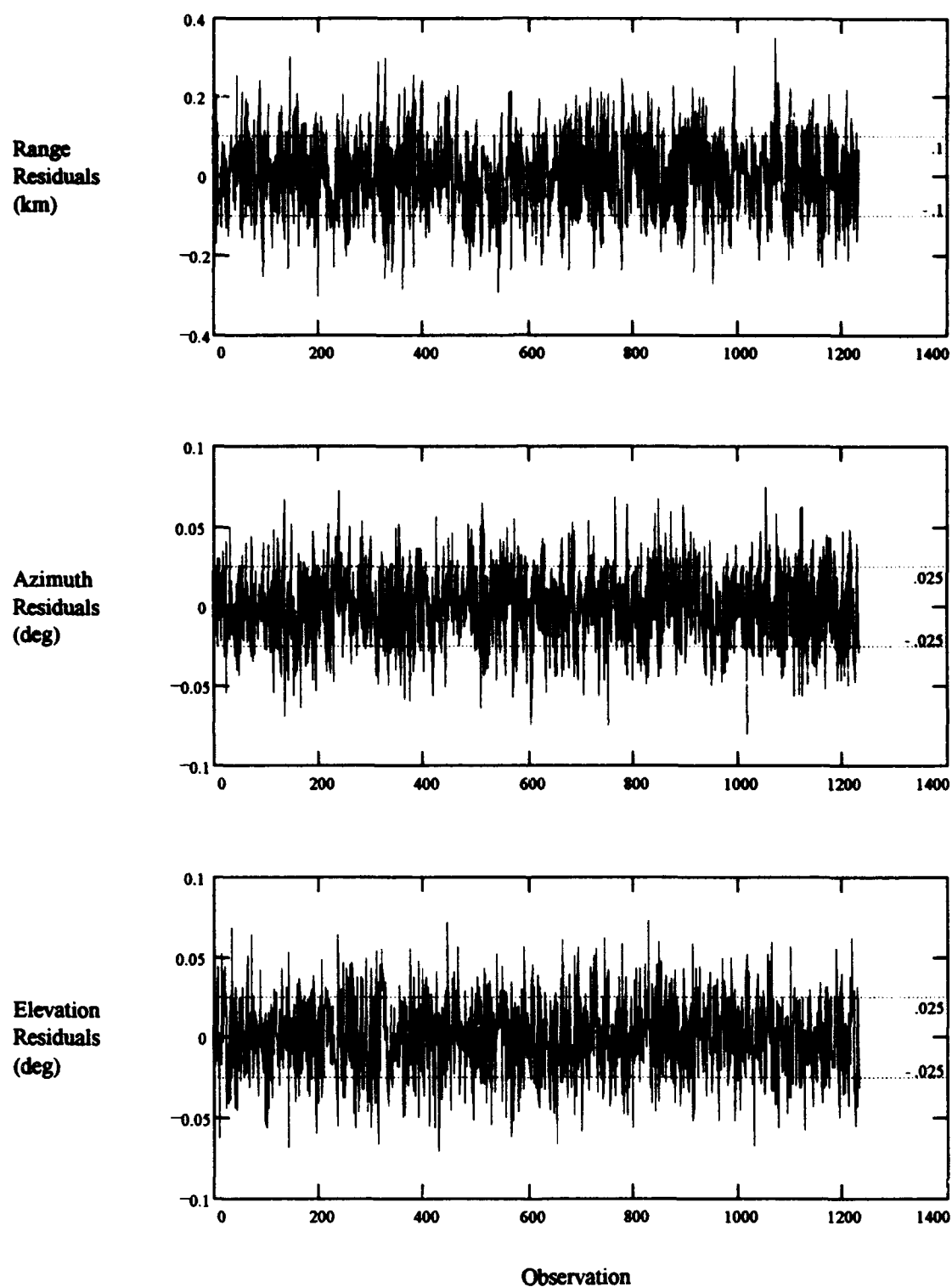


Figure 23. Residual Values versus One Sigma After Convergence - Low El Pass

4.3.2 Accuracy of Estimate. The estimator's accuracy is evaluated by comparing the estimated state for each pass to the true state and calculating the position and velocity error vector magnitudes. Figure 24 plots the position and velocity errors versus maximum elevation for the low orbit (satellite 20003) for both the high and low data rates. As expected, the accuracy of the estimated state improves as the maximum pass elevation increases and as the data rate increases. The improvement is most rapid at the lower elevations and seems to level off at the higher elevations. This is because of the non-linear relationship between maximum elevation and track duration. Breaking the plots in Figure 24 into three zones: Zone 1 accounts for an average of 58% of the total change in error magnitude, Zone 2 accounts for about 28% of the total change, and Zone 3 accounts for the remaining 14%.

Figure 25 plots the position and velocity errors versus maximum elevation for the high orbit (satellite 20004) for both the high and low data rates. Again, the accuracy of the estimate improves with increasing elevation and data rate and the improvement is still most rapid at low elevations.

When using the low data rate, the plot of error magnitude versus elevation results in fairly smooth curves. However, the higher data rate results in curves with very different behavior. Accuracy improves rapidly until the elevation reaches about 10 degrees. The accuracy then *decreases* until the elevation reaches 15-20 degrees after which it again improves. This behavior is most noticeable in the velocity errors and is most pronounced for the high orbit. In general, the accuracy of the estimate is better for the low orbit than for the high orbit. Position errors are consistently about 10-16 meters higher for the high orbit. The velocity errors show a much larger degree of variability. At elevations less than 10 degrees, the velocity errors for the high orbit are actually *less* than for the low orbit. Between 16-35 degrees, the velocity errors for the high orbit are about 50% greater than for the low orbit. For elevations above 50 degrees, the velocity errors for the high and low orbits vary by less than 10%. Figure 26 graphically compares the errors for the high and low orbits.

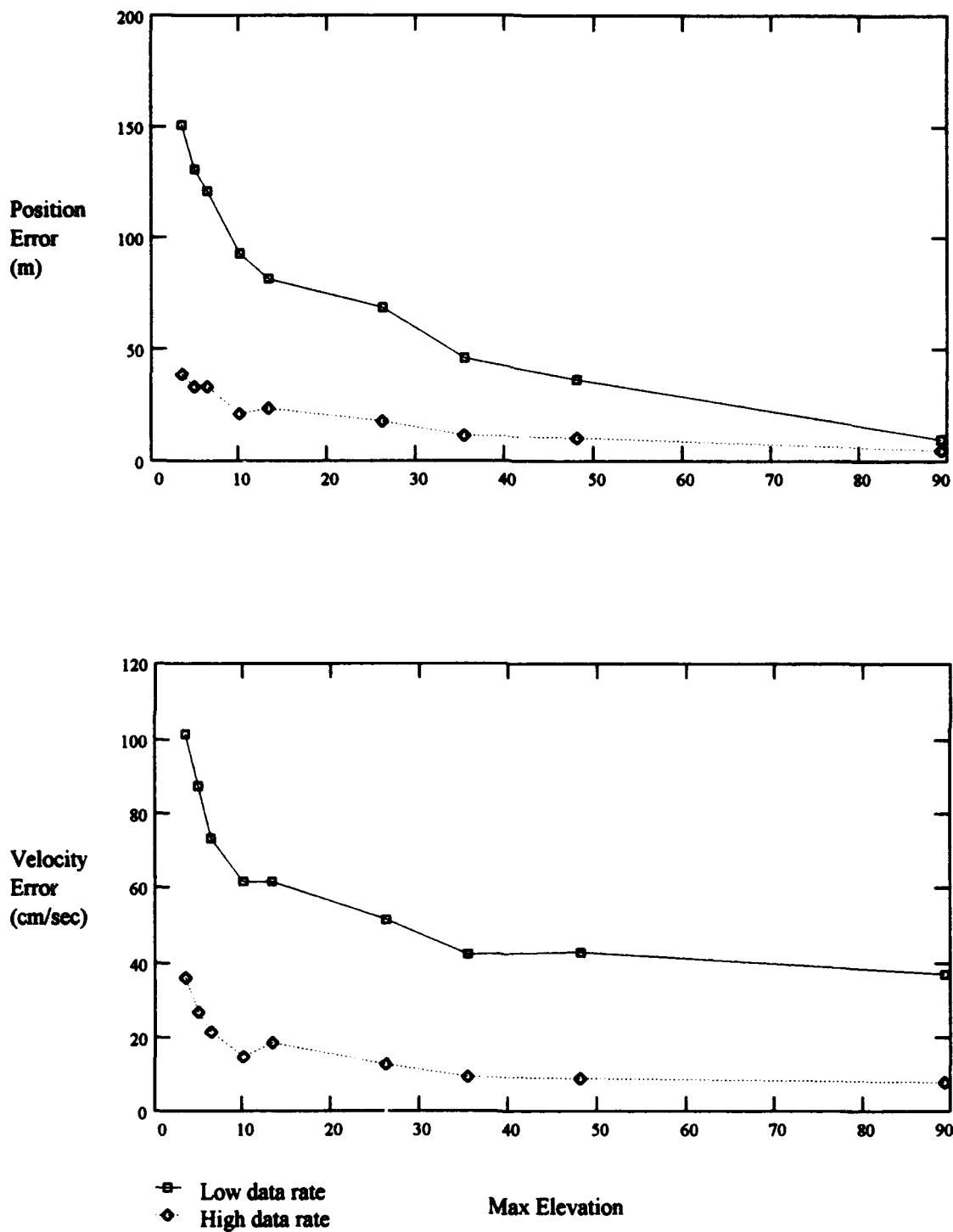


Figure 24. Position and Velocity Errors versus Max Elevation - Low Orbit

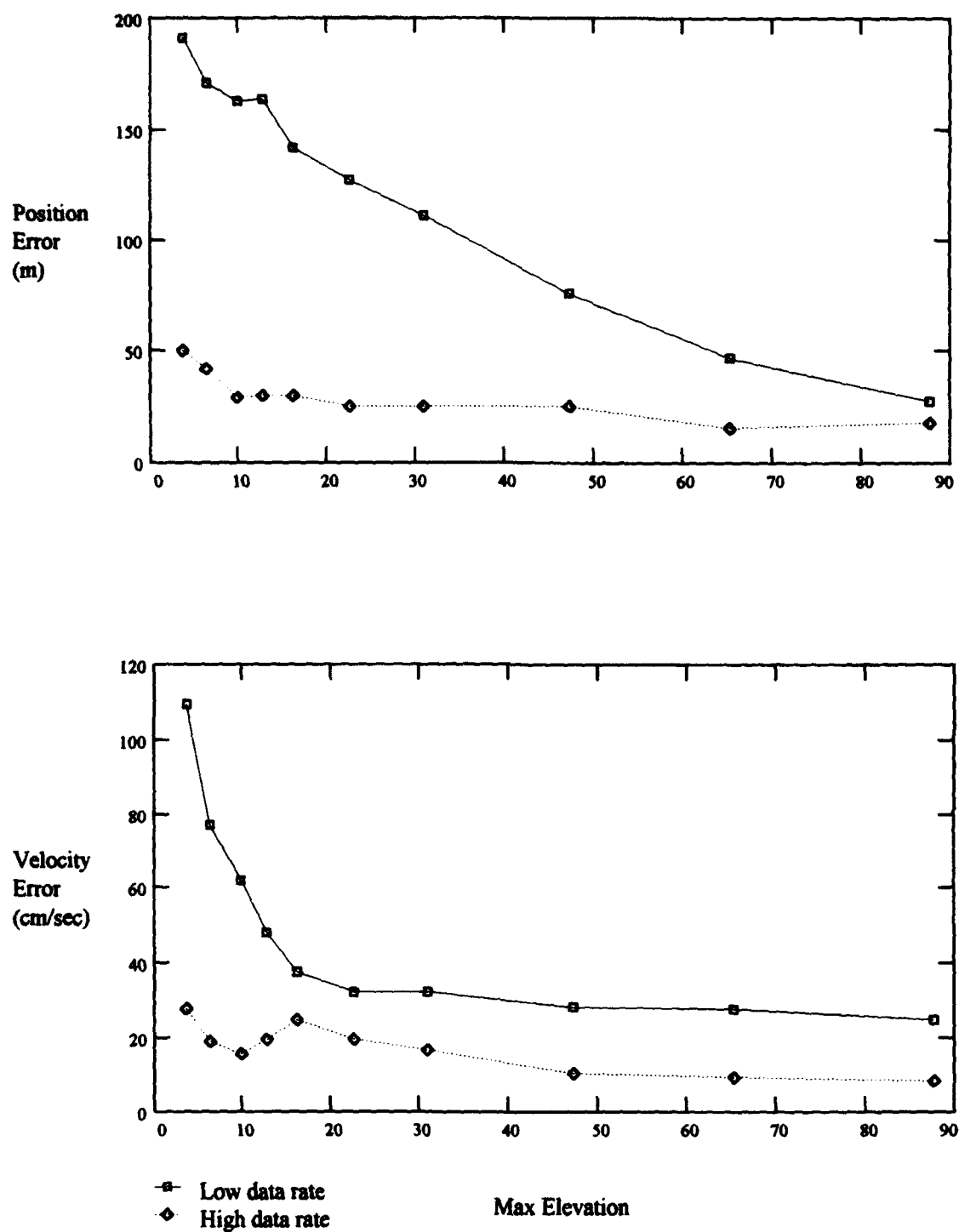


Figure 25. Position and Velocity Errors versus Max Elevation - High Orbit

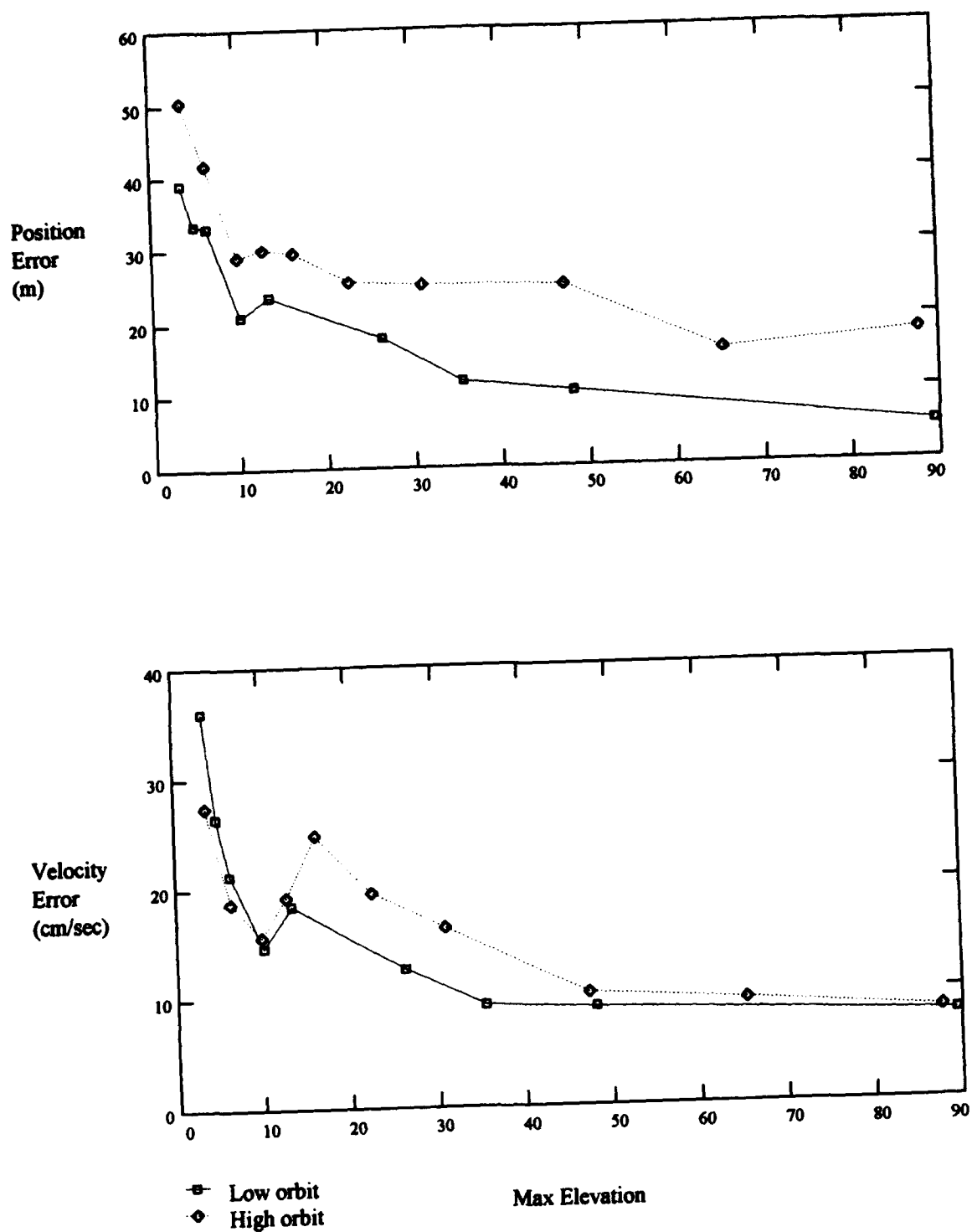


Figure 26. Position and Velocity Errors versus Max Elevation - High Data Rate

4.3.3 *Covariance Matrix.* The analysis in the previous section was possible only because the true state was a known quantity from the truth model. In reality, the true state is usually not known and so some other way of assessing the quality of the estimate is necessary. This can be found in the covariance matrix which is generated during the estimation process.

Using the state covariance matrix it is possible to calculate the covariance associated with the position and velocity errors (4:43). The first step is to write an expression relating the error to the state vector. Next calculate the gradient of this expression with respect to the state vector. Now the gradient and state transition matrix can be combined to find the variance in each error:

$$\sigma_{err}^2 = \nabla R^T \mathbf{P}_{state}(t_0) \nabla R \quad (57)$$

where R is the scalar expression relating the position or velocity error magnitude to the state vector and $\mathbf{P}_{state}(t_0)$ is the state covariance matrix associated with the estimate.

Table 11 compares the standard deviation in position and velocity (as predicted by the covariance matrix) with the actual average errors for six different pass profiles. The estimator does a good job of estimating the variance (which is merely the square of the standard deviation) for position but is very optimistic when estimating the variance for velocity.

Table 11. Comparison of Predicted and Actual Estimator Accuracy

Orbit	Pass Elevation	σ_{r-err}	avg $_{R-err}$	avg $_{R-err} / \sigma_r$	σ_{v-err}	avg $_{v-err}$	avg $_{v-err} / \sigma_v$
Low	3.5	35.979	38.933	1.082	4.479	35.989	8.035
"	35.4	11.077	11.497	1.038	0.749	9.254	12.355
"	89.4	4.682	4.983	1.064	0.547	7.916	14.472
High	3.65	47.305	50.449	1.067	5.887	27.411	4.656
"	22.41	18.821	25.446	1.352	3.116	19.533	6.269
"	87.78	3.53	17.7	5.014	0.452	8.294	18.350

The estimator is slightly optimistic in calculating the variance in position for most passes, but as the track durations become very long it seems to become more and more optimistic. This can be seen in the last two rows of Table 11. This probably indicates that the track lengths are beginning to exceed the span over which the approximate equations of state give a good fit with reality.

Estimates of the variance for velocity are very optimistic and differ from the actual errors by an order of magnitude on average. Both high and low orbits show increasingly optimistic estimates of the variance as the track length increases. Interestingly, the estimator generally does a better job with the higher orbit although the effect of track length mentioned before seems to be manifesting itself in the last pass profile. The most likely reason for the overly optimistic estimate for the velocity variance is that the velocity terms in the equations of state were only developed to the fourth order while the position terms were developed to the fifth order.

4.4 Summary

The analysis was begun with four different estimators to test different orders of approximation in the equations of state and state transition matrix. Measures of estimator performance were compiled using noise-less or "perfect" observations. Based on these results, only one of the estimators was chosen for further analysis. When given observation data that included gaussian noise, the fifth order estimator effectively extracted all of the pertinent information from the data and provided accurate estimates of position and velocity.

V. Conclusions and Recommendations

5.1 Introduction

The analysis of Chapter 4 shows that a differential corrector based on Taylor Series approximations of the equations of state and state transition matrix can adequately estimate the state for near earth orbits. The key element in the success of the estimator was the use of a sufficient number of terms in the approximate equations.

5.2 Conclusions

The number of terms in the Taylor Series equations of state required to properly model the orbital dynamics is ultimately driven by the expected track duration. This is because the Taylor Series is an expansion in time. As the time span over which the equations must operate increases (i.e. longer tracks), additional terms must be added to the equations or they will fail to properly model the dynamics. Although the fifth order estimator appears to perform well for the two orbits studied, it would probably begin to perform poorly as the orbital altitude increases since altitude is a major factor in track length.

As expected, the two body effect is the dominant term in the state and the state transition matrix equations. However, although small, the effect of the J_2 geopotential term is noticeable for these low earth orbits and therefore the estimator dynamics needs to take this into account. This does not mean that the estimator will not work without the J_2 term in the dynamics -- only that it will not work quite as well.

Estimator performance is much more sensitive to the order of the equations of state than to the order of the state transition matrix. This is demonstrated by the difference in performance between 'ets5' and 'ets4b'. Both use the same state transition matrix equations but 'ets5' has equations of state one order higher than those of 'ets4b' (see Table 2 and section 4.2).

As expected, the accuracy of the estimator was related to the number of available observations. The higher data rate resulted in consistently more accurate estimates than the lower data rate. As the track length increased due to increasing maximum pass elevation the accuracy of the estimate also increased.

Accuracy was also affected by orbit altitude and tended to be better for the lower orbit. This was probably due to reduced effectiveness of the approximate equations over the longer time spans generated by the higher orbit.

Two effects can be seen to be working against each other. Longer track lengths mean more data is available for the estimator and so the accuracy of the estimate is better. However, longer track lengths also mean longer time spans. As noted before, the use of approximate equations for the dynamics means that the effectiveness of the dynamics model decreases with increasing time span. So one effect works to improve the estimate while the other works to degrade the estimate.

As developed in this study, the estimator's covariance matrix provides overly optimistic estimates of the accuracy of the estimated velocity. The most likely explanation for this is that the state and state transition matrix equations for velocity are one order lower than the equations for position.

5.3 Recommendations

It should be possible to improve the accuracy of the covariance matrix by improving the velocity equations to be of the same order as the position equations. This should be done for both the equations of state and the state transition matrix. Only additional terms for the two-body effect would need to be added because of the relatively small effect of J_2 .

The order of the Taylor Series approximations should probably be increased to sixth order or possibly higher. This is because the performance of the fifth order estimator is expected to degrade when orbits higher than those looked at in this study must be estimated. Note that the highest orbit in this study has a period of 110 minutes while the definition of Near Earth includes satellites with periods up to 225 minutes.

Consider using a numerical integrator to propagate the state and state transition matrix instead of a Taylor Series approximation. Not only would the calculation of the state and state transition matrix be more exact, but the problem of an effective *interval of convergence* associated with using approximate equations would be eliminated. Also, the major reason for using approximate equations was to reduce processing time since numerical integrators are usually very computationally intensive. However, as the

order of the approximate equations increases, the equations become quite complex and lose their time saving advantage over numerical integration.

5.4 Potential Areas of Study

Additional testing on different orbits should be done. Higher altitude orbits should be looked at to determine if additional terms are needed in the Taylor Series approximations for the equations of state and state transition matrix. Other orbital aspects such as inclination and eccentricity should also be investigated. Of special interest would be orbits with inclinations of 90 and 63.4 degrees since these orbits minimize the J_2 effect on rotation of the line-of-nodes and line-of-apsides respectively.

Further analysis on the effect of drag on the estimator's accuracy should also be done. This could be done by repeating the same sequence of data runs done for this study but using truth data that does not include drag effects. The results could then be compared and the drag effects determined.

Investigation of the "cup" seen in the velocity errors near the 10 degree maximum pass elevation could be done to explain why this occurred. Also, additional passes could be analyzed to better characterize the relationship between pass elevation and estimator performance.

The estimator could be rewritten to use a numerical integrator instead of the Taylor Series approximations for the state and state transition matrix equations. Of primary interest would be whether this would improve the accuracy of the estimate and its associated covariance matrix as well as eliminating the interval of convergence problem.

One of the basic premises of this study is that the output from the estimator can be grouped with other similar estimates to solve for other perturbations such as drag. Development of a batch or sequential estimator to use this data to produce elsets similar to those currently produced by the SSC should be undertaken. Analysis of this "master" estimator should probably focus on: (1) obtaining good estimates of drag, (2) generating elsets compatible with and comparable to those produced by the SSC, (3) determining if SSN performance would be improved by using this approach.

Currently the SSC is not really set up to use a state vector and covariance matrix as input to their estimator (known as 'SGP4'). Therefore it might be useful to see if the state vector could be converted to a form more readily used by the SSC algorithms.

5.5 Summary

This study demonstrated that a least squares estimator using approximate equations for the state and state transition matrix can effectively and accurately estimate the state of a Near Earth satellite using observations from a ground based space surveillance radar. Some limitations of the estimator used in the study and ways to correct or eliminate them were also identified. Further areas of study were suggested to fill in gaps that could not be fully covered in this study. Of special note was the increasing complexity in the approximate equations required to handle longer and longer sensor tracks and the potential of using a numerical integrator to eliminate this problem.

Appendix A. Coordinate Frame Transformations

A.1 Determining LMST and Site ECI Coordinates

At any given time the earth will have a certain orientation relative to the ECI coordinate axes. The Greenwich mean sidereal time (GMST) specifies the angle along the celestial equator (measured eastward) between the mean equinox and the Greenwich meridian. The GMST for any arbitrary time is

$$\theta_g = 100.4606184 + 36000.77004J + 0.000387933J^2 + 360.98564724 \frac{UT}{24} \quad (58)$$

where θ_g is the GMST in degrees, J is the number of Julian centuries from Julian year 2000.0, and UT is the universal time in hours (8: 21, 23). The Julian century can be calculated from

$$J = \frac{J_0 - 2451545.0}{36525} \quad (59)$$

where J_0 is the value of the Julian date at 0^h UT (8: 21). Once the GMST is known, the site's *local mean sidereal time* (LMST) can be calculated as $\theta = \theta_g + \Lambda$, where Λ is the site's east longitude. Figure 27 shows graphically the relationship between the mean equinox, GMST, and LMST.

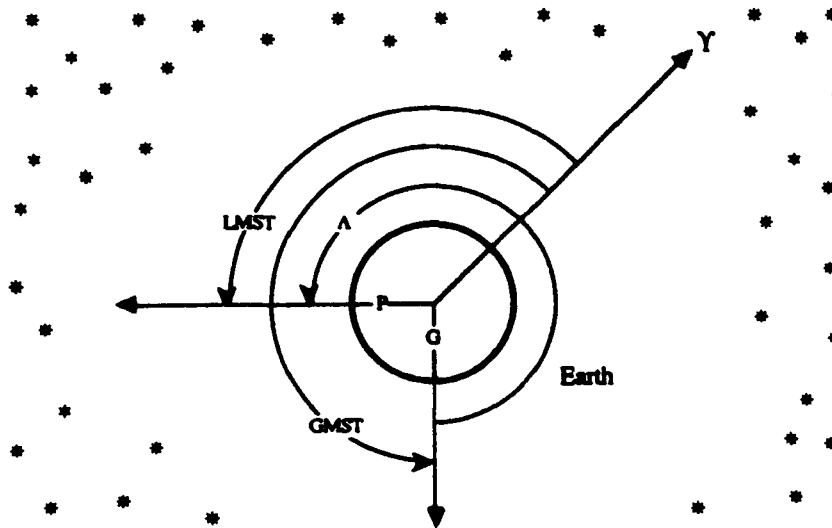


Figure 27. Relationship between Mean Equinox, GMST, and LMST (8: 23)

The earth can be modeled as an oblate spheroid with an ellipsoidal cross section. The semi-major axis lies along the earth's equatorial radius and the semi-minor axis is the earth's polar radius (2: 93). Since the cross section through the equator is still circular the longitude of a sensor site is unchanged. However, by using this model the determination of the latitude of a site on the earth's surface is more complex and leads to the definitions of *geocentric* and *geodetic* latitudes. As can be seen in Figure 28, geocentric (L') and geodetic (L) latitudes are quite different. When the latitude for a site is given, it is usually the geodetic latitude that is meant (2: 94). The reference ellipsoid used in this model has the following dimensions: Equatorial radius (a_e) = 6378.145 km, Polar radius (b_e) = 6356.785 km, and Eccentricity (e) = 0.08182 (2:94).

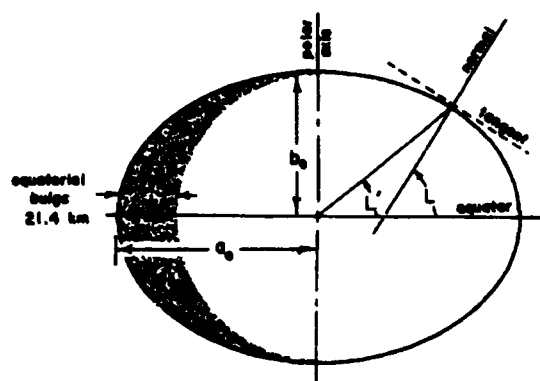


Figure 28. Geocentric and geodetic latitude (2: 95)

If the equatorial axis is labeled "x" and the polar axis is labeled "z", then the rectangular coordinates of a site will be

$$\begin{aligned} x &= \left| \frac{a_e}{\sqrt{1-e^2 \sin^2 L}} + h \right| \cos L \\ z &= \left| \frac{a_e(1-e^2)}{\sqrt{1-e^2 \sin^2 L}} + h \right| \sin L \end{aligned} \quad (60)$$

where a_e is the earth's equatorial radius, e is the earth's eccentricity, L is the geodetic latitude, and h is the site's elevation above sea level (2: 98). When combined with the LMST, the site's location in ECI coordinates is

$$\bar{\mathbf{R}} = x \cos \theta \hat{\mathbf{I}} + x \sin \theta \hat{\mathbf{J}} + z \hat{\mathbf{K}} \quad (61)$$

A.2 Earth Centered Inertial (ECI) to Topocentric Transformation

Once the site's inertial coordinates are known the satellite's position relative to the site is computed as:

$$\mathbf{dr} = \mathbf{r}_{\text{sat}} - \mathbf{r}_{\text{site}} \quad (62)$$

where \mathbf{dr} is the satellite's relative position, \mathbf{r}_{sat} is the satellite's position in ECI coordinates, and \mathbf{r}_{site} is the site's location in ECI coordinates. The satellite's relative position is then converted to the SEZ frame using:

$$\begin{aligned} \rho_s &= x \sin \lambda \cos \theta + y \sin \lambda \sin \theta - z \cos \lambda \\ \rho_e &= y \cos \theta - x \sin \theta \\ \rho_z &= x \cos \lambda \cos \theta + y \cos \lambda \sin \theta + z \sin \lambda \end{aligned} \quad (63)$$

where ρ_s , ρ_e , ρ_z are the components of the relative position vector in the SEZ frame, x , y , z are the components of the relative position vector found in Eq (61), λ is the site's latitude, and θ is the LMST for the site at the time of the observation. The SEZ vector is finally converted to the topocentric coordinates by:

$$\begin{aligned} \text{range} &= \rho = \sqrt{x^2 + y^2 + z^2} \\ \text{elevation} &= \beta = \text{asin}(\rho_z / \rho) \\ \text{azimuth} &= \text{acos} \left(\frac{-\rho_s}{\sqrt{\rho_s^2 + \rho_e^2}} \right) \end{aligned} \quad (64)$$

A.3 Topocentric to ECI Transformation

Converting from topocentric coordinates to ECI coordinates is basically the reverse of going from ECI to topocentric. The first step is still to find the site's inertial location. Once that is done the topocentric coordinates are transformed into the SEZ frame:

$$\begin{aligned}\rho_z &= -\rho \cos\beta \cos\alpha \\ \rho_e &= \rho \cos\beta \sin\alpha \\ \rho_s &= \rho \sin\beta\end{aligned}\tag{65}$$

The next step is to convert from SEZ coordinates to ECI coordinates using:

$$\begin{aligned}dx &= \rho_s \sin\lambda \cos\theta - \rho_e \sin\theta + \rho_z \cos\lambda \cos\theta \\ dy &= \rho_s \sin\lambda \sin\theta + \rho_e \cos\theta + \rho_z \cos\lambda \sin\theta \\ dz &= \rho_s \cos\lambda + \rho_z \sin\lambda\end{aligned}\tag{66}$$

where dx , dy , and dz are the components for the relative position vector between the site and the satellite expressed in ECI coordinates. The final step then is to add the relative position vector and the site location together:

$$\mathbf{r}_{sat} = \mathbf{r}_{site} + d\mathbf{r}\tag{67}$$

Appendix B. The Data Linearization Matrix, H

The data linearization matrix is given by Eq (18) as:

$$\mathbf{H} = \frac{\partial \mathbf{G}}{\partial \mathbf{x}}(\mathbf{x}_{ref}(t_i), t_i) \quad (18)$$

For a satellite orbiting the earth, the observation relation \mathbf{G} is:

$$\mathbf{G} = \begin{pmatrix} \rho \\ az \\ el \end{pmatrix} = \begin{pmatrix} \sqrt{\rho_s^2 + \rho_e^2 + \rho_z^2} \\ \pi - a \tan(\rho_z / \rho_s) \\ a \tan(\rho_z / \sqrt{\rho_s^2 + \rho_e^2}) \end{pmatrix} \quad (68)$$

where ρ , az , el are the range, azimuth and elevation components of the topocentric observation vector and ρ_s , ρ_e , ρ_z are the SEZ components of the topocentric observation vector. In the SEZ topocentric frame, the satellites position is:

$$\bar{\rho}_{SEZ} = \mathbf{D}(\mathbf{r} - \mathbf{R})_{ECI} \quad (69)$$

where \mathbf{r} is the satellite's position in ECI coordinates, \mathbf{R} is the site's position in ECI coordinates and \mathbf{D} is the rotation matrix from the ECI frame to the SEZ frame:

$$\mathbf{D} = \begin{bmatrix} \sin \lambda \cos \theta & \sin \lambda \sin \theta & -\cos \lambda \\ -\sin \theta & \cos \theta & 0 \\ \cos \lambda \cos \theta & \cos \lambda \sin \theta & \sin \lambda \end{bmatrix} \quad (70)$$

where λ is the site's latitude and θ is the site's LMST.

Since \mathbf{G} is linearized with respect to the state vector, the site position can be ignored and so

$$\delta \bar{\rho}_{SEZ} = \mathbf{D} \delta \mathbf{r} \quad (71)$$

and

$$\delta \mathbf{z} = \frac{\partial \mathbf{G}_{topo}}{\partial \bar{\rho}_{SEZ}} \delta \bar{\rho}_{SEZ} = \mathbf{H}_1 \mathbf{D} \delta \mathbf{r} \quad (72)$$

where z is the observation vector range, azimuth and elevation. Changes in the observation vector are linearly related to changes in the satellites state as:

$$\delta z = H \delta x \quad (73)$$

and so Eq (72) can be rewritten and solved for H as:

$$H = H_1 D \quad (74)$$

since $\delta r / \delta x = 1$.

After differentiating the equations in Eq (68) the result is:

$$H_1 = \begin{bmatrix} \frac{\rho_s}{\rho} & \frac{\rho_e}{\rho} & \frac{\rho_z}{\rho} \\ \frac{\rho_e}{\rho_s^2 + \rho_e^2} & \frac{-\rho_s}{\rho_s^2 + \rho_e^2} & 0 \\ \frac{-\rho_s \rho_z}{\rho^2 \sqrt{\rho_s^2 + \rho_e^2}} & \frac{-\rho_e \rho_z}{\rho^2 \sqrt{\rho_s^2 + \rho_e^2}} & \frac{\sqrt{\rho_s^2 + \rho_e^2}}{\rho^2} \end{bmatrix} \quad (75)$$

Appendix C. State Transition Matrix, Φ

The state transition matrix, commonly denoted by Φ , is found by taking the gradient of the equations of state evaluated at the initial conditions. When the equations of state are available in explicit form this relationship can be expressed as:

$$\Phi(t, t_0) = \nabla_{\mathbf{x}(t_0)} \mathbf{h}(\mathbf{x}(t_0), t) \quad (14)$$

where $\mathbf{x}(t_0)$ is the state at the initial or reference conditions and \mathbf{h} is the relationship that relates the state at t_0 to the state at any other time t .

In this study the equations of state are explicit expressions obtained from a Taylor Series expansion of the equations of motion. As can be seen in Section 3.3.2, Eqs (48, 51-56), these equations are rather large and complex, so the easiest way to derive the Φ matrix is to develop it term by term and then add all the parts together. For notational purposes, each term in the development will be denoted as Φ_{sub} , where the subscript refers to the order of the term. The same notation is used when referencing a particular term in the Taylor Series (such as \mathbf{h}_0 which would be the zero term in the series). Also, all quantities are evaluated at the reference or initial conditions.

C.1 The Two-body Terms

The zero order term is:

$$\Phi_0 = \nabla_{\mathbf{x}} \mathbf{h}_0 = \nabla \begin{pmatrix} \mathbf{r} \\ \mathbf{v} \end{pmatrix} = \mathbf{I} \quad (76)$$

where \mathbf{r} , \mathbf{v} are the initial position and velocity vectors and \mathbf{I} is a 6x6 identity matrix.

The first order term is:

$$\Phi_1 = \nabla \mathbf{h}_1 = \nabla \begin{pmatrix} \mathbf{v} \\ \mathbf{a} \end{pmatrix} dt = \begin{bmatrix} \mathbf{0} & \mathbf{I} \\ \mathbf{A} & \mathbf{0} \end{bmatrix} dt \quad (77)$$

where \mathbf{a} is the initial acceleration vector (reference Eq (53)), $\mathbf{0}$ is a 3x3 null matrix, \mathbf{I} is a 3x3 identity matrix and \mathbf{A} is the 3x3 matrix:

$$\mathbf{A} = \mu \begin{bmatrix} (3x^2/r^5 - 1/r^3) & 3xy/r^5 & 3xz/r^5 \\ 3xy/r^5 & (3y^2/r^5 - 1/r^3) & 3yz/r^5 \\ 3xz/r^5 & 3yz/r^5 & (3z^2/r^5 - 1/r^3) \end{bmatrix} \quad (78)$$

where μ is the earth's gravitational parameter, x, y, z are the position coordinates of the state in the ECI frame of reference, and r is the magnitude of the position vector.

The second order term is:

$$\Phi_2 = \nabla \mathbf{h}_2 = \nabla \frac{1}{2} \begin{pmatrix} \mathbf{a} \\ \dot{\mathbf{a}} \end{pmatrix} dt^2 = \frac{1}{2} \begin{bmatrix} \mathbf{A} & \mathbf{0} \\ \mathbf{B} & \mathbf{C} \end{bmatrix} dt^2 \quad (79)$$

where $\dot{\mathbf{a}}$ is the first time derivative of the acceleration vector (see Eq (51)), the 3x3 matrix \mathbf{B} is:

$$\mathbf{B} = \mu \begin{bmatrix} [15(\mathbf{r} \cdot \mathbf{v})x^2/r^2 - 3(\mathbf{r} \cdot \mathbf{v}) - 6ux]/r^5 & [15(\mathbf{r} \cdot \mathbf{v})xy/r^2 - 3vx - 3uy]/r^5 & [15(\mathbf{r} \cdot \mathbf{v})xz/r^2 - 3wx - 3uz]/r^5 \\ [15(\mathbf{r} \cdot \mathbf{v})xy/r^2 - 3vx - 3uy]/r^5 & [15(\mathbf{r} \cdot \mathbf{v})y^2/r^2 - 3(\mathbf{r} \cdot \mathbf{v}) - 6vy]/r^5 & [15(\mathbf{r} \cdot \mathbf{v})yz/r^2 - 3wy - 3vz]/r^5 \\ [15(\mathbf{r} \cdot \mathbf{v})xz/r^2 - 3wx - 3uz]/r^5 & [15(\mathbf{r} \cdot \mathbf{v})yz/r^2 - 3wy - 3vz]/r^5 & [15(\mathbf{r} \cdot \mathbf{v})z^2/r^2 - 3(\mathbf{r} \cdot \mathbf{v}) - 6wz]/r^5 \end{bmatrix} \quad (80)$$

and the 3x3 matrix \mathbf{C} is:

$$\mathbf{C} = \mu \begin{bmatrix} -(1/r^3 - 3x^2/r^5) & 3xy/r^5 & 3xz/r^5 \\ 3xy/r^5 & -(1/r^3 - 3y^2/r^5) & 3yz/r^5 \\ 3xz/r^5 & 3yz/r^5 & -(1/r^3 - 3z^2/r^5) \end{bmatrix} \quad (81)$$

The third order term is:

$$\Phi_3 = \nabla \mathbf{h}_3 = \nabla \frac{1}{6} \begin{pmatrix} \ddot{\mathbf{a}} \\ \ddot{\dot{\mathbf{a}}} \end{pmatrix} dt^3 = \frac{1}{6} \begin{bmatrix} \mathbf{B} & \mathbf{C} \\ -\mu \mathbf{D} & \mathbf{E} \end{bmatrix} dt^3 \quad (82)$$

where $\ddot{\mathbf{a}}$ is given by Eq (52) and the 3x3 matrix \mathbf{D} is:

$$\begin{aligned}
\mathbf{D}(1,1) &= -105(\mathbf{rdv})^2 x^2 / r^9 - 3\mu x^2 / r^8 + [15(\mathbf{rdv})^2 + 60(\mathbf{rdv})ux + 15x^2 (\text{vel}^2 - \mu / r)] / r^7 \\
&\quad - \mu / r^6 - [6u^2 + 3(\text{vel}^2 - \mu / r)] / r^5 + 6\mu x^2 / r^4 \\
\mathbf{D}(1,2) &= [30(\mathbf{rdv})(vx + uy) + 15xy(\text{vel}^2 - \mu / r)] / r^7 - 6uv / r^5 - 9\mu xy / r^8 - 105(\mathbf{rdv})^2 xy \\
\mathbf{D}(1,3) &= [30(\mathbf{rdv})(wx + uz) + 15xz(\text{vel}^2 - \mu / r)] / r^7 - 6uw / r^5 - 9\mu xz / r^8 - 105(\mathbf{rdv})^2 xz \\
\mathbf{D}(2,1) &= \mathbf{D}(1,2) \\
\mathbf{D}(2,2) &= -105(\mathbf{rdv})^2 y^2 / r^9 - 3\mu y^2 / r^8 + [15(\mathbf{rdv})^2 + 60(\mathbf{rdv})vy + 15y^2 (\text{vel}^2 - \mu / r)] / r^7 \\
&\quad - \mu / r^6 - [6v^2 + 3(\text{vel}^2 - \mu / r)] / r^5 + 6\mu y^2 / r^4 \\
\mathbf{D}(2,3) &= [30(\mathbf{rdv})(wy + vz) + 15yz(\text{vel}^2 - \mu / r)] / r^7 - 6vw / r^5 - 9\mu yz / r^8 - 105(\mathbf{rdv})^2 yz \\
\mathbf{D}(3,1) &= \mathbf{D}(1,3) \\
\mathbf{D}(3,2) &= \mathbf{D}(2,3) \\
\mathbf{D}(3,3) &= -105(\mathbf{rdv})^2 z^2 / r^9 - 3\mu z^2 / r^8 + [15(\mathbf{rdv})^2 + 60(\mathbf{rdv})wz + 15z^2 (\text{vel}^2 - \mu / r)] / r^7 \\
&\quad - \mu / r^6 - [6w^2 + 3(\text{vel}^2 - \mu / r)] / r^5 + 6\mu z^2 / r^4
\end{aligned} \tag{83}$$

where $\text{vel} = |\mathbf{v}|$ and $\mathbf{rdv} = (\mathbf{r} \cdot \mathbf{v})$.

The \mathbf{E} matrix is given by:

$$\mathbf{E} = -\frac{\mu}{r^5} \begin{bmatrix} 30(\mathbf{r} \cdot \mathbf{v})x^2 / r^2 - 6(\mathbf{r} \cdot \mathbf{v}) - 12ux & 30(\mathbf{r} \cdot \mathbf{v})xy / r^2 - 6vx - 6uy & 30(\mathbf{r} \cdot \mathbf{v})xz / r^2 - 6wx - 6uz \\ 30(\mathbf{r} \cdot \mathbf{v})xy / r^2 - 6vx - 6uy & 30(\mathbf{r} \cdot \mathbf{v})y^2 / r^2 - 6(\mathbf{r} \cdot \mathbf{v}) - 12vy & 30(\mathbf{r} \cdot \mathbf{v})yz / r^2 - 6wy - 6vz \\ 30(\mathbf{r} \cdot \mathbf{v})xz / r^2 - 6wx - 6uz & 30(\mathbf{r} \cdot \mathbf{v})yz / r^2 - 6wy - 6vz & 30(\mathbf{r} \cdot \mathbf{v})z^2 / r^2 - 6(\mathbf{r} \cdot \mathbf{v}) - 12wz \end{bmatrix} \tag{84}$$

The fourth order term (which was only calculated for position) is:

$$\Phi_4 = \nabla \mathbf{h}_4 = \nabla \frac{1}{24} \begin{pmatrix} \ddot{\mathbf{a}} \\ 0 \end{pmatrix} dt^4 = \frac{1}{24} \begin{bmatrix} \mathbf{D} & \mathbf{E} \\ \mathbf{0} & \mathbf{0} \end{bmatrix} dt^4 \tag{85}$$

C.2 The J_2 Terms

Following the same procedure used for the two-body elements of the Φ matrix, the first order term for J_2 effects is:

$$\Phi_{J1} = \nabla \begin{pmatrix} 0 \\ \mathbf{a}_{20} \end{pmatrix} dt = \begin{bmatrix} \mathbf{0} & \mathbf{0} \\ \mathbf{F1} & \mathbf{0} \end{bmatrix} dt \tag{86}$$

where \mathbf{a}_{20} is given by Eq (55) and the 3x3 matrix $\mathbf{F1}$ is:

$$\mathbf{F1} = -A \begin{bmatrix} 3/r^5 - 15(x^2 + z^2)/r^7 + 105x^2z^2/r^9 & -15xy/r^7 + 105xyz^2/r^9 & -45xz/r^7 + 105xz^3/r^9 \\ -15xy/r^7 + 105xyz^2/r^9 & 3/r^5 - 15(y^2 + z^2)/r^7 + 105y^2z^2/r^9 & -45yz/r^7 + 105yz^3/r^9 \\ -45xz/r^7 + 105xz^3/r^9 & -45yz/r^7 + 105yz^3/r^9 & 9/r^5 - 90z^2/r^7 + 105z^4/r^9 \end{bmatrix} \quad (87)$$

The second order term is:

$$\Phi_{12} = \nabla \frac{1}{2} \begin{pmatrix} \mathbf{a}_{20} \\ \dot{\mathbf{a}}_{20} \end{pmatrix} dt^2 = \begin{bmatrix} \mathbf{F1} & \mathbf{0} \\ -A\mathbf{F2} & \mathbf{F3} \end{bmatrix} dt^2 \quad (88)$$

where A is the quantity defined in Eq (39), $\dot{\mathbf{a}}_{20}$ is given by Eq (56), and the 3x3 matrix $\mathbf{F2}$ is:

$$\begin{aligned} \mathbf{F2}(1,1) &= [-30ux - 2wz - (rdv)]/r^7 - 945xz^3(rd\dot{v})/r^{11} \\ &\quad + 105[uz^3 + 2wx^2z + uxz^2 + x^2(rd\dot{v})]/r^9 \\ \mathbf{F2}(1,2) &= -15(vx + uy)/r^7 - 945yz^3(rd\dot{v})/r^{11} \\ &\quad + 105[vz^3 + y(2wxz + uz^2 + x(rd\dot{v}))]/r^9 \\ \mathbf{F2}(1,3) &= -45(uz + wx)/r^7 - 945z^4(rd\dot{v})/r^{11} \\ &\quad + 105z[wz^2 + 3z(rd\dot{v}) + 2wxz + uz^2 + x(rd\dot{v})]/r^9 \\ \mathbf{F2}(2,1) &= -15(vx + uy)/r^7 - 945xz^3(rd\dot{v})/r^{11} \\ &\quad + 105[uz^3 + y(2wyz + vz^2 + y(rd\dot{v}))]/r^9 \\ \mathbf{F2}(2,2) &= [-30vy - 2wz - (rdv)]/r^7 - 945yz^3(rd\dot{v})/r^{11} \\ &\quad + 105[vz^3 + 2wy^2z + vyz^2 + y^2(rd\dot{v})]/r^9 \\ \mathbf{F2}(2,3) &= -45(vz + wy)/r^7 - 945z^4(rd\dot{v})/r^{11} \\ &\quad + 105z[wz^2 + 3z(rd\dot{v}) + 2wyz + vz^2 + y(rd\dot{v})]/r^9 \\ \mathbf{F2}(3,1) &= -45(uz + wx)/r^7 - 945xz^3(rd\dot{v})/r^{11} \\ &\quad + 105[uz^3 + 3x(wz^2 + z(rd\dot{v}))]/r^9 \\ \mathbf{F2}(3,2) &= -45(vz + wy)/r^7 - 945yz^3(rd\dot{v})/r^{11} \\ &\quad + 105[vz^3 + 3y(wz^2 + z(rd\dot{v}))]/r^9 \\ \mathbf{F2}(3,3) &= -[180wz + 45(rd\dot{v})]/r^7 - 945z^4(rd\dot{v})/r^{11} \\ &\quad + 210[2wz^3 + 3z^2(rd\dot{v})]/r^9 \end{aligned} \quad (89)$$

using the same notation as Eq (83). The 3x3 **F3** matrix is:

$$\mathbf{F3} = -A \begin{bmatrix} 3/r^5 - 15(x^2 + z^2)/r^7 + 105xz^3/r^9 & -15xy/r^7 + 105yz^3/r^9 & -45xz/r^7 + 105z^4/r^9 \\ -15xy/r^7 + 105xz^3/r^9 & 3/r^5 - 15(y^2 + z^2)/r^7 + 105yz^3/r^9 & -45yz/r^7 + 105z^4/r^9 \\ -45xz/r^7 + 105xz^3/r^9 & -45yz/r^7 + 105yz^3/r^9 & 9/r^5 - 90z^2/r^7 + 105z^4/r^9 \end{bmatrix} \quad (90)$$

The third order term is:

$$\Phi_{J3} = \nabla \frac{1}{6} \begin{pmatrix} \dot{\mathbf{a}}_{20} \\ 0 \end{pmatrix} dt^3 = \begin{bmatrix} -A\mathbf{F2} & \mathbf{F3} \\ 0 & 0 \end{bmatrix} dt^3 \quad (91)$$

The final Φ matrix is then:

$$\Phi(dt) = \Phi_0 + \Phi_1 + \Phi_2 + \Phi_3 + \Phi_4 + \Phi_{J1} + \Phi_{J2} + \Phi_{J3} \quad (92)$$

As was done for the equations of state, the equations for position are essentially one order higher than the velocity equations. Of special interest is the fact that as higher order terms are added to the matrix their derivatives become very large and complex and increasingly difficult to derive.

Bibliography

1. "Mechanics, Celestial." *Encyclopaedia Britannica*. 1977 ed.
2. Bate, Roger R., Mueller, Donald D., and White, Jerry E. *Fundamentals of Astrodynamics*. New York: Dover Publications, Inc., 1971.
3. Gauss, Karl Friedrich. *Theory of the Motion of the Heavenly Bodies Moving About the Sun in Conic Sections*. A translation of *Theoria Motus* (1857) by Charles H. Davis. New York, Dover Publications, Inc., 1963.
4. Wiesel, William E., Jr. Class handout distributed in MECH 731, Modern Methods of Orbit Determination. School of Engineering, Air Force Institute of Technology (AU), Wright-Patterson AFB OH, March 1993.
5. Carnahan, Brice, and others. *Applied Numerical Methods*. New York, John Wiley & Sons, Inc., 1969.
6. Wiesel, William E., Jr. Class handout distributed in MECH 636, Advanced Astrodynamics. School of Engineering, Air Force Institute of Technology (AU), Wright-Patterson AFB OH, January 1993.
7. Macko, Stanley J. *Satellite Tracking*. New York, John F. Rider Publisher, Inc., 1962.
8. National Aeronautics and Space Administration. *The 1976 Standard Atmosphere Above 86-km Altitude*. NASA SP-398. Washington, 1976.
9. Markley, Landis F. "Approximate Cartesian State Transition Matrix" *Journal of the Astronautical Sciences*, Vol 34, No 2: 161-169 (April-June 1986).
10. Roehrich, Ronald L. Senior Engineer, HQ USSPACECOM/ANS, Peterson AFB, CO. Telephone interview. 21 October 1993.

Vita

Captain Garry L. Hall was born on 16 March 1961 in Roanoke, Virginia. He graduated from Northside High School in Roanoke County, Virginia in 1979 and attended Virginia Polytechnic Institute and State University, graduating with a Bachelor of Science in Aerospace and Ocean Engineering in December 1983. Upon graduation, he was commissioned in the USAF and served his first tour of duty at Wright-Patterson AFB, Ohio as a System Safety Engineer on both the AGM-65 "Maverick" and the Advanced Cruise Missile (ACM) programs. Upon volunteering for the BEST program, he was assigned to the 16 SURS (Cobra Dane) Shemya AFB, Alaska as a Space Surveillance Crew Commander from August 1987 to August 1988. Afterwards, he served at HQ USSPACECOM/J3SO, first as a Space Surveillance Center Deputy Commander/Orbital Analyst and then in a staff capacity as the Chief Orbital Analyst and J3SO Security Manager. As the Chief Orbital Analyst, Captain Hall supervised over 20 other Orbital Analysts in support of USSPACECOM's mission to detect, track, analyze and report all space events. In May 1992, Captain Hall entered the Graduate School of Engineering at the Air Force Institute of Technology.

Permanent Address: 8131 Otterview Dr .
Roanoke, VA 24019

REPORT DOCUMENTATION PAGE

Form Approved
GMB No. 2704-0138

This report contains information which has been determined to be releasable under the provisions of the President John F. Kennedy Assassination Records Collection Act of 1992 (Public Law 102-361). This information is being made available to the public in accordance with the provisions of the Act. The information is being made available to the public in accordance with the provisions of the Act. The information is being made available to the public in accordance with the provisions of the Act.

1. AGENCY USE ONLY (Leave blank)		2. REPORT DATE March 1994	3. REPORT TYPE AND DATES COVERED Master's Thesis	
4. TITLE AND SUBTITLE COMPRESSION OF A RADAR TRACK OF A NEAR EARTH SATELLITE INTO AN EARTH CENTERED INERTIAL STATE VECTOR USING LEAST SQUARES DIFFERENTIAL CORRECTION			5. FUNDING NUMBERS	
6. AUTHOR(s) Garry L. Hall, Captain, USAF			8. PERFORMING ORGANIZATION REPORT NUMBER AFIT/GA/EN/94M-1	
7. PERFORMING ORGANIZATION NAME(S) AND ADDRESS(ES) Air Force Institute of Technology, WPAFB OH 45433-6583			10. SPONSORING MONITORING AGENCY REPORT NUMBER	
9. SPONSORING MONITORING AGENCY NAME(S) AND ADDRESS(ES) Lt Col Salvatore Alfano, USAF PL/VTA 3550 Aberdeen Ave., SE Kirtland AFB, NM 87117-6008			11. SUPPLEMENTARY NOTES	
12a. DISTRIBUTION AVAILABILITY STATEMENT Approved for public release; distribution unlimited			12b. DISTRIBUTION CODE	
13. ABSTRACT (Maximum 200 words) This study investigated the use of a least squares differential corrector to compress the information contained in a single radar track of a Near Earth satellite into a six element, Earth Centered Inertial state vector and associated covariance matrix. Observations were generated using a truth model program based on two-body, J2 geopotential, and atmospheric drag dynamics and consisted of simulated range, azimuth and elevation. Random Gaussian noise was added to the data to simulate real world random errors. The orbital dynamics used in the estimator consisted of two-body and J2 geopotential effects which were approximated using a Taylor Series expansion in time. Analysis was conducted using two circular, inclined low earth orbits. Estimator performance was evaluated as a function of maximum pass elevation, track duration, data rate and the order of approximation of the equations of state. The estimator successfully extracted all of the pertinent information from the data with accuracy being dependent on the number of data points available. A correlation between the required order of approximation and maximum expected track length was also noted.				
14. SUBJECT TERMS Orbit Estimation, Least Squares, Taylor Series Equations, Orbital Mechanics, Satellite Tracking			15. NUMBER OF PAGES 91	
			16. PRICE CODE	
17. SECURITY CLASSIFICATION OF REPORT Unclassified	18. SECURITY CLASSIFICATION OF THIS PAGE Unclassified	19. SECURITY CLASSIFICATION OF ABSTRACT Unclassified	20. LIMITATION OF ABSTRACT UL	